CEBAF Program Advisory Committee Ten Proposal Cover Sheet

This document must be received by close of business on Tuesday, December 19, 1995 at:

CEBAF
User Liaison Office, Mail Stop 12 B
12000 Jefferson Avenue
Newport News, VA 23606

(Choose one)

☒ **New Proposal Title:** Photon Asymmetry in $^{3}He(\vec{\gamma},\pi^{+})^{3}H$

☐ **Update Experiment Number:**

☐ **Letter-of-Intent Title:**

Contact Person

Name: Blaine Norum
Institution: University of Virginia
Address: Department of Physics
Address: University of Virginia
City, State ZIP/Country: Charlottesville, VA 22901
Phone: (804) 924-6789 **FAX:** (804) 924-4576
E-Mail → Internet: ben@virginia.edu

Experimental Hall: B **Days Requested for Approval:** 28

CEBAF Use Only

Receipt Date: 12/19/95 PR 95-004

By: gp

BEAM REQUIREMENTS LIST

CEBAF Proposal No.: _____ Date: _____
(For CEBAF User Liaison Office use only)

List all combinations of anticipated targets and beam conditions required to execute the experiment. (This list will form the primary basis for the Radiation Safety Assesment Document (RSAD) calculations that must be performed for each experiment.)

Condition #	Beam Energy (MeV)	Beam Current (μA)	Polarization and Other Special Requirements (e.g., time structure)	Target Material (use multiple rows for complex targets — e.g., w/windows)	Target Material Thickness (mg/cm²)
1	4500	2.5	Unpolarized	^{3}He	1000
				mylar	50

The beam energies, E_{Beam}, available are: $E_{Beam} = N \times E_{Linac}$ where N = 1, 2, 3, 4, or 5. For 1995, E_{Linac} = 800 MeV, i.e., available E_B 800, 1600, 2400, 3200, and 4000 MeV. Starting in 1996, in an evolutionary way (and not necessarily in the order given) the fol additional values of E_{Linac} will become available: E_{Linac} = 400, 500, 600, 700, 900, 1000, 1100, and 1200 MeV. The sequen timing of the available resultant energies, E_{Beam}, will be determined by physics priorities and technical capabilities.

HAZARD IDENTIFICATION CHECKLIST

CEBAF Experiment: _____ Date: _____

Check all items for which there is an anticipated need—do not check items that are p of the CEBAF standard experiment (HRSE, HRSH, CLAS, HMS, SOS in stand configurations).

Cryogenics
- _____ beamline magnets
- _____ analysis magnets
- X target
- _____ drift chambers
- _____ other

Electrical Equipment
- _____ cryo/electrical devices
- _____ capacitor banks
- _____ high voltage
- _____ exposed equipment

Radioactive/Hazardous Materi
List any radioactive or hazadoro toxic materials planned for use:
_____
_____

Pressure Vessels
- _____ inside diameter
- _____ operating pressure
- _____ window material
- _____ window thickness

Saclay L^3He Target

Flammable Gas or Liquids
(incl. target)
type: _____
flow rate: _____
capacity: _____

Other Target Materials
- ___ Beryllium (Be)
- ___ Lithium (Li)
- ___ Mercury (Hg)
- ___ Lead (Pb)
- ___ Tungsten (W)
- ___ Uranium (U)
- ___ Other (list below)

_____
_____

Vacuum Vessels
- _____ inside diameter
- _____ operating pressure
- _____ window material
- _____ window thickness

Radioactive Sources
- _____ permanent installation
- _____ temporary use

type: _____
strength: _____

Large Mech. Structure/System
- _____ lifting devices
- _____ motion controllers
- _____ scaffolding or elevate platforms
- _____ other

Lasers
type: Argon-ion
wattage: 10 W
class: IV

Installation
- X permanent
- _____ temporary

Use
- _____ calibration
- _____ alignment

photon source

Hazardous Materials
- ____ cyanide plating materials
- ____ scintillation oil (from)
- ____ PCBs
- ____ methane
- ____ TMAE
- ____ TEA
- ____ photographic developers
- ____ other (list below)

_____
_____
_____

Notes:
_____
_____
_____
_____
_____
_____

Photon Asymmetry in $^3\mathrm{He}(\vec{\gamma}, \pi^+)^3\mathrm{H}$

H. Baghaei, A. Cichocki, T. Gresko, D. Higinbotham, V. Gladyshev,
R. A. Lindgren, B. E. Norum, C. Smith, and K. Wang
University of Virginia, Charlottesville, Virginia

H. Crannell, S. Matthews, J. O'Brian, D. Sober
Catholic University of America, Washington, DC

J. Chen, J. Mitchell, and E. Smith
CEBAF, Newport News, Virginia

C. Bennhold, W. Briscoe, P. Cole, and K. Dhuga
George Washington University, Washington, D.C.

H. Weller
Duke University, Durham, NC

R. Ent and C. Keppel
Hampton University, Hampton, Virginia

C. Berisso, R. S. Hicks, R. A. Miskimen,
J. Shaw, and G. A. Peterson
University of Massachusetts, Amherst, MA

J. R. Calarco
University of New Hampshire, Durham, New Hampshire

T. P. Welch
Oregon State University, Corvallis, Oregon

D. Beatty, T. Fortune, W. Lorenzon, and J. Yu
University of Pennsylvania, Philadelphia, PA

J. Napolitano and P. Stoler
Rensselaer Polytechnic Institute, Troy, NY

AND THE REAL PHOTON GROUP OF CLAS

December, 1995, PAC 10 CEBAF

Abstract

We propose to study the reaction $^3He(\vec{\gamma},\pi^+)^3H$ with the momentum transfer Q^2 ranging up to 20 fm^{-2} using polarized photons from 300 MeV to 650 MeV. Both the differential cross section and the photon asymmetry Σ will be measured. The broad kinematic range spanned by the data will enable us to investigate a possible breakdown of DWIA (arising from two-body mechanisms and possible changes in elementary amplitudes), the influence of two-step processes in a dense nuclear system, and the magnitude of D-state components in the nuclear three-body wave function. Of these, the principal focus will be on the possible breakdown of the Impulse Approximation arising from modifications of the $E_{1+}(\Delta)$ amplitude in a dense nuclear system. The existence of a D-wave admixture in the trinucleon wave function gives rise to potentially large SD interference contribution to Σ. This contribution is approximately proportional to the $E_{1+}(\Delta)$ amplitude so the photon asymmetry Σ provides a sensitive measure of the $E_{1+}(\Delta)$ amplitude. The experiment will require the unique combination of properties provided by the CLAS detector and the proposed Compton $\vec{\gamma}$ source.

1 Introduction

A principal goal of nuclear physics is to understand how nucleons and nucleonic processes are affected by the presence of other nucleons in a nuclear medium. To study this question amplitudes for a process involving a nucleus are compared to those for the corresponding process on a free nucleon. The results of such comparisons can be sensitive to several distinct effects. In the case of charged pion photoproduction these include the presence of meson-exchange or other two-body currents in the nucleus, pion-nucleus rescattering, details of the nuclear wave function, final state interactions between the outgoing pion and residual nucleus, and possible differences in the elementary amplitudes. The magnitude of the effect of each of these depends upon the kinematics of a particular measurement and upon the observable being measured: total cross section (σ), differential cross section ($d\sigma/d\Omega$), photon asymmetry (Σ), etc. If the contributions for all but one of these effects are known for a particular measurement, then that measurement can yield new information about the remaining effect.

One question that can be addressed in this manner relates to the properties of the nucleonic resonances. Total photoabsorption data from Frascati[24] indicate that excitation of the Δ resonance appears to be unaffected by whether the nucleon involved is in a nucleus or not. By contrast, the higher resonances such as the D_{13} which appear prominantly in photoabsorption on the proton are washed out completely in photoabsorption on a nucleus. This can be understood qualitatively by noting that the Δ excitation is dominated by the M_{1+} spin-flip amplitude whereas the higher resonances correspond to spatial excitations. The amplitude for flipping the spin of one quark should, to first approximation, be independent of changes in the spatial wave function whereas the amplitude for a quadrupole excitation, for example, would be very sensitive. It follows that if one wants to look for nuclear medium effects on the Δ excitation process one should look at the quadrupole component, the E_{1+} amplitude. The photon asymmetry Σ in the reaction $^3He(\vec{\gamma},\pi^+)^3H$ is particularly sensitive to this amplitude; examining this amplitude is, therefore, the principal focus of the proposed experiment. Other effects, such as the presence of meson-exchange or other two-body currents, pion-nucleus rescattering, and final state interactions between the outgoing pion and residual nucleus will also be studied both for the need to control them in order to isolate the effect of the E_{1+} amplitude as well as for their own intrinsic

interest.

The ^{3}He nucleus is an ideal target for such studies. It is the simplest nucleus wherein the nucleons are bound tightly together and the nuclear structure is well understood. Precise, correlated three-body wave functions can be obtained using, for example, the Faddeev approach calibrated to electron scattering and other data. Consequently, interpreting the data in terms of the nuclear structure contributions is very reliable. This is in contrast to the case for heavier nuclei where the single particle wave functions are computed using the the shell, or other similarly phenomenological models in which effective nuclear structure parameters are constrained by β-decay rates, electromagnetic form factors, and other experimental observables. In these cases, ambiguities are inevitable, especially in magnetic transitions. In order to isolate reliably the effects of interest from the effects of nuclear structure it is necessary to know the both the initial and final nuclear states. The most effective way to do this is to require that the recoiling nucleons stay integrated as ^{3}H. Thus, with respect to isospin the reaction is essentially an "elastic" or "iso-elastic" process as opposed to an "inelastic" process wherein the ^{3}He is broken apart.

The earliest experimental study of the $^3He(\gamma,\pi^+)^3H$ reaction was performed in the 1960's [2] at the University of Illinois with 180 MeV to 260 MeV photons produced by bremsstrahlung radiation. The measured cross sections were found to be generally well described by impulse approximation. However, when examined in detail, the cross section were observed to lie from 25 to 50% below the simple theory. The discrepancy was attributed to the inaccurate wave functions and a suppression of pion production in nuclear matter.

Another experiment was performed using a bremsstrahlung beam at Saclay in the 1970's [3]. The differential cross sections could be described at small momentum transfers by the impulse approximation with Feddeev wave functions. However, as the momentum transfer was increased above 6 fm^{-2}, a discrepancy between the data and a calculation using the distorted-wave impulse approximation (DWIA) appeared. A complete calculation with a novel two-body contribution was required to give a full description [4] of the data. Significantly, this two-body formalism predicts that at higher photon energies, such as 400 MeV and above, the two-body contribution constitutes almost the entire cross section.

Subsequently, the measurement was repeated at Saclay but this time using

a positron-annihilation photon source which provided quasi-monochromatic photons [5]. Besides the iso-elastic process, two-body and three-body break up channels were also studied. The energy of the photon beam was from 210 MeV to 450 MeV. The angles at which pions were detected ranged from 20° to 72°, corresponding to momentum transfers from 0.28 fm^{-2} to 3.0 fm^{-2}. For the data at higher momentum transfer calculations including the two-step charge-exchange process, $^3He(\gamma,\pi^0)^3He(\pi^0,\pi^+)^3H$, gave a better description.

The experiment was also performed at Bonn using the bremsstrahlung beam of the 500 MeV synchrotron [6]. The recoiling nuclei were detected in coincidence with the produced pion permitting a relatively clean isolation of the iso-elastic process. The cross sections in these measurements were found to be lower than the theoretical calculations indicating that the understanding of the reaction is incomplete.

Theoretical work on this reaction was initially performed within the framework of the plane-wave impulse approximation(PWIA) [7]. These calculations were followed by DWIA calculations [8] which included the pion rescattering contribution. Later calculations by Laget [9] explicitly included both real and imaginary components in both the M_{1+} and E_{1+} multipoles. Most recently, Kamalov, Tiator and Bennhold [1] (KTB) have carried out a general study of polarization observables for this reaction. The calculations were performed within a newly developed coupled-channels framework [8] that can consistently describe elastic π^+ and coherent π^0 photoproduction as well as elastic and charge-exchange pion scattering on ^{3}He. The KTB calculation successfully reproduced the cross section of the $^3He(\gamma,\pi^+)^3H$ data over a wide range of photon energies and momentum transfers. The most attractive parts of the calculation are the single polarization observables Σ (photon asymmetry), T (target polarization asymmetry) and P (recoil polarization asymmetry). These polarization observables contain interference terms of the various reaction amplitudes in different combinations and may be more sensitive to small amplitudes of interesting dynamic effects. With a polarized photon beam much more information on the dynamics of the system can be extracted than is possible with unpolarized beams. The KTB calculation predicts that some small components, such as the D-wave component in the ^3He wave function, can drastically affect polarization observables. The calculations showed that the photon asymmetry Σ is very sensitive to details of the trinucleon wave function (such as D-state components) and the E_{1+} amp-

litude of the delta. Consequently, a study of the $^3He(\vec{\gamma},\pi^+)^3H$ reaction will enable us to access important issues inaccessible using unpolarized photons.

Until recently, the full capabilities of the photon as a probe of nuclear systems have not been realizable due to technical limitations. While high fluxes of high energy, unpolarized photons have been available from a variety of bremsstrahlung sources similar fluxes of polarized photons have not. During the last few years polarized photon beams obtained from both bremsstrahlung and Compton backscattering sources have become available. Unfortunately, in the case of bremsstrahlung sources the polarization is significant only for a relatively narrow range of photon energies at about $\frac{1}{3}$ to $\frac{1}{2}$ of the maximum photon energy. In addition, the degree of polarization is modest $\approx$ 50%, although this can be increased at the expense of energy range and tagging efficiency. Existing and most planned Compton backscattering sources are operated as parasitic operations at synchrotron light sources.[23] Consequently, while they have the very desirable properties of high polarization at the highest photon energies, very high tagging efficiency, and a broad range of energies at which the polarization is significant, their fluxes are very limited by constraints on how many electrons they can remove from the rings. Also, the energy resolution of these beams is poor, ranging from about 5.5 MeV at LEGS to an expected 15 MeV at GRAAL.

We plan to perform measurements of the differential cross sections and photon polarization asymmetries in Hall B using the proposed Compton backscattering facility [11], the liquid ^3He target designed by the Saclay group [12], and the CLAS. The proposed Compton backscattering source in Hall B of CEBAF will have the advantages of existing Compton backscattering facilities but without the limitations. It will be able to deliver an intense, highly polarized beam possessing excellent energy resolution, very little background radiation, and very few untagged $\vec{\gamma}$'s. In its initial configuration the source will be based on an Ar-ion laser capable of delivering 10 W of 514 nm at a single frequency. The light will be stored in a high gain (amplification 33,000) Fabry-Perot cavity. Scattering the light from a 4.5 GeV electron beam will generate polarized photons at energies up to 650 MeV. The source will have an unmatched figure of merit $\mathcal{F}_m$ given by

$$\mathcal{F}_m = N_\gamma < P_\gamma^2 > \eta \qquad (1)$$

are required, where $< P_\gamma^2 >$ is the average photon polarization over some range of photon energies and η is the tagging efficiency. A resolution of 2

MeV in the photon energy will be achieved using the tagging spectrometer with a new, dedicated detector. The two-body kinematics of the Compton scattering process strictly limits the maximum energy of the γ 's so there will be essentially no untagged, high energy photons; the kinematics also generate an energy-angle correlation in the γ 's enabling us to strictly exclude photons with energies below the range of interest by collimation. Finally, since there is no material target in the beam the level of background radiation will be very low.

The CLAS will permit detection of π^+'s emitted between 10° to 120°. With the anticipated momentum resolution, the iso-elastic peak will be clearly separable from the two- and three-body break up channels. At higher energies and backward π^+ production angles, it will also be possible to detect the recoiling ^3H. This will completely suppress all other backgrounds under those kinematic conditions where the cross section is the smallest. The excellent track reconstruction properties of the CLAS will enable us to use a long target, thereby maximizing the luminosity and counting rate. Significantly, the small transverse dimensions of the $\vec{\gamma}$ beam will enable us to use a target with a small transverse extent, thereby minimizing the material through which reaction products must pass and minimizing the degradation of track reconstruction capabilities that results from multiple scattering.

These technologies are ideally suited to this measurement. This combination of photon beam, detector, and target make Hall B at CEBAF the only place at which this experiment is feasible.

2 Physics Motivation

The most important quantity to be measured is the polarized photon asymmetry, defined by

$$\Sigma = \frac{d\sigma/d\Omega^{\perp} - d\sigma/d\Omega^{\parallel}}{d\sigma/d\Omega^{\perp} + d\sigma/d\Omega^{\parallel}}$$

where the superscript $\perp$ ($\parallel$) refers to photons linearly polarized perpendicular (parallel) to the reaction plane. In a very simple model based on an harmonic-oscillator S-shell nuclear wave function, the photon asymmetry for $^3He(\vec{\gamma},\pi^+)^3H$ and a nucleon process $p(\vec{\gamma},\pi^+)n$ can be related simply by

$$\Sigma(^3He) = \Sigma(p)$$

However this is true only for a naive model in which only the S-wave component in the ^3He wave functions is considered. In a realistic model, the D-wave component can drastically affect this equality. The most extensive calculation of this quantity for the reaction $^3He(\vec{\gamma},\pi^+)^3H$ has been carried out by Kamalov, Tiator, and Bennhold [1]. In calculating Σ a trinucleon wave function in momentum space is used. It is dominated by the S-state amplitude (90%) while the D-state contributes about 8%. If only the major S-wave components and the lowest pion-nucleon s- and p-waves in the amplitude $t_{\gamma N}$ are considered, the photon asymmetry can be expressed in terms of the multipoles $E_{l\pm}$ and $M_{l\pm}$ as

$$\Sigma_S = \frac{\pi sin^2\Theta}{d\sigma_A/d\Omega}[M^2_{000}(Q)|2M_{1+} + M_{1-}|^2 - \frac{1}{3}M^2_{101}(Q)|f_{em}|^2]W_A, \qquad (2)$$

where W_A is a kinematic factor,

$$f_{em} = 3E_{1+} - M_{1+} + M_{1-}$$

and $M_{SLJ}(Q)$ are nuclear form factors, S and L are the spin and orbital angular momentum of the pair-nucleon inside the trinucleon system, and J is the angular momentum transfer in the scattering process, with $J = 0$ for non-spin-flip and J=1 for spin-flip processes.

When the D-wave component is included, additional contributions to the photon asymmetry arise, one important part coming from the interference

between the S- and D-state components. The KTB theory offers an explicit expression for this contribution at $\Theta_{c.m.} = 90^o$ in terms of the elementary multipoles:

$$\Sigma_{SD}(90^o) = \frac{\sqrt{2}\pi}{Q^2 d\sigma_A/d\Omega} M_{101}(Q) M_{121}(Q)[2qk\Re E_{0+} f^*_{em} - q^2|E_{0+}|^2 - (4k^2+q^2)|f_{em}|^2]W_A \quad (3)$$

where q and k are the momentum of the pion and photon respectively and Q is the momentum transfer. The SD interference term contains a large E_{0+} multipole, which does not exist in an S-wave function. Therefore, an enhancement of D-state contribution will lead to a drastic modification of the photon asymmetry. The first term in the square brackets in equation 3 gives an interference of E_{0+} and E_{1+} multipoles due to the presence of a D-state component. This interference will increase the sensitivity of the photon asymmetry to the E2(Δ) transition. It should be noted that this effect is rather small in the differential cross section due to the large background produced by the E_{0+} and M_{1+} multipoles.

The E_{0+} appearing here is that for charged pion production. It is, of course, much larger than that for π^0 production and is the reason that we use charged pion production to study Δ properties rather than the more commonly used π^0 production.

Figure 1 shows the results of a PWIA calculation in which the contribution from different components are compared. As the photon energy increases, the contribution of the D-state component in ^{3}He becomes larger and the photon asymmetry even changes sign at $E_\gamma = 450 MeV$. Also shown in figure 1 is the PWIA calculation using full elementary amplitude without the $E2(\Delta)$ transition in the $\gamma N\Delta$ vertex. The KTB theory predicts that the sensitivity of the photon asymmetry to the $E2(\Delta)$ transition is enhanced when using the full wave function in contrast to using only the S-state components. Hence, the D-wave configuration enhances the effect of the E_{1+} multipole as expected as well as the role of the $E2(\Delta)$ transition.

The KTB theory uses a coupled-channel calculation to account for the final state interaction (FSI). The largest contribution of the two-step process $(\gamma,\pi^0)(\pi^0,\pi^+)$ comes from the coherent non-spin-flip transition in the (γ,π^0) channel with subsequent spin-flip transition in the (π^0,π^+) channel. Therefore, the spin degrees of freedom in the pion-nuclear interaction significantly affect polarization observables in charged-pion photoproduction at backward angles.

Comparisons of different calculations of the differential cross sections and photon asymmetries are shown in figure 2. The KTB results are computed in PWIA (dashed curves), in DWIA (dash-dotted curves) with no two-step processes, and the coupled-channel formalism (solid curves) which incorporates the contribution from the $^3He(\gamma,\pi^0)^3He(\pi^0,\pi^+)^3H$ process. There are several noteworthy features in the comparisons. First, the complete treatment of FSI generates much improved agreement between measured and calculated cross sections at $E_\gamma = 300$ MeV. Second, although pion rescattering well reproduced the cross section, there is little influence on photon asymmetry at forward angles ($\Theta_{c.m.} < 50°$). Third, at larger angles, pion rescattering has a larger effect on photon asymmetry. Figures 3 and 4 show the corresponding angular dependencies for a photon energy of 520 MeV.

Figure 5 shows the KTB prediction of photon asymmetry at a small angle, $\Theta_{c.m.} = 30°$ as a function of the photon energy. In this region, the influence of pion rescattering is small. Using S-state components from a the three-body Faddeev wave function or from an harmonic oscillator S-shell wave function gives similar results. This is because the momentum transfer is small at forward angles and the D-wave contribution is necessarily small. For the same reason, the sensitivity to the $E_{1+}(\Delta)$ is weak. However, by comparing the dotted curve to the others, it can be seen that Δ-isobar inside the nuclear medium gives a sizable contribution[14]. Figure 6 shows the corresponding predictions for $\Theta_{c.m.} = 30°$.

Figure 7 shows the energy dependence at $\Theta_{c.m.} = 90°$ of the differential cross section and photon asymmetry from a coupled-channel calculation. Obviously, the D-wave components and the $E_{1+}(\Delta)$ multipoles cause a drastic change. The photon asymmetry is less than 0.2 for small photon energies but increases to a maximum for photon energies around 350 MeV to 400 MeV. The smaller partial waves reduce Σ by up to 30% and leaves a detectable signature. As E_γ increases beyond 350 MeV, the KTB calculation shows a large variation when the $E_{1+}(\Delta)$ multipole is or is not included; it enhances the photon asymmetry at 400 MeV by more than a factor of two.

In examining the disagreement between the experimental and theoretical cross sections, Kamalov *et al.*[4] developed a two-body mechanism which reproduces the data. PWIA works well for low momentum transfers, but as Q^2 increases to $6fm^{-2}$ the agreement worsens and it can not be recovered by including pion rescattering. The introduced two-body mechanism, arising mainly from the isovector magnetic components of the two-body operator,

raises the cross section by up to two orders of magnitude. Figure 8 shows both existing data and the theoretical predictions. At 400 MeV and 120°, a factor of 10 times enhancement due to the inclusion of the two-body mechanism can be observed.

It must be noted here that DWIA calculations for photon energies beyond 520 MeV are not currently available due to technical difficulties with the computations; the number of partial waves required becomes excessive and the computations become numerically unstable. The calculation of distortion effects at higher energies will require use of a Glauber or Eikonal approach and is being pursued. Nevertheless, one can extrapolate the effects of adding distortions at lower energies to get an idea of what can be expected. Basically, one sees the structures in Σ shifted to higher photon energies. The insensitivity of Σ to the E_{1+} amplitude observed at 520 MeV in the plane wave calculation can be expected to reappear at 600-650 MeV in a full DWIA treatment.

In summary, potentially rich physics is contained in the combination of precise cross section and photon asymmetry measurements. With a polarized photon beam and a large acceptance detector it will be possible to study this physics by measuring the photon asymmetry over a wide range of energies and angles. The cross section data at all energies and angles will enable us to determine the effects of distortions, two-body currents, and multistep processes. The photon asymmetry data for photon energies of 600-650 MeV (where the E_{1+} amplitude is expected to play little or no role) will provide a crucial consistency check. Measurements of Σ at lower photon energies will permit a determination of the E_{1+} amplitude in a nuclear system. It is expected that by the time this experiment is performed the E_{1+} amplitude on the free nucleon will be precisely known. Our results then will provide a sensitive measure of the effect of the nuclear medium on the Δ.

3 Experimental Approach

The proposed experimental study of photon asymmetry in $^3He(\vec{\gamma},\pi^+)^3H$ will require a polarized photon source, a large acceptance detector with good resolution, and a cryogenic liquid ^3He target. This section will be devoted to a discussion of the photon source, the CLAS detector, the target, and a Monte Carlo simulation of the experiment.

3.1 Photon Beam, ^{3}He Target, and Detector

The proposed Compton $\vec{\gamma}$ source in Hall B of CEBAF[11] will provide a beam uniquely suited to a measurement of the photon asymmetry in pion photoproduction from ^{3}He. Polarized γ's with energies up to about 650 MeV will be produced by the Compton backscattering of laser light from the 4.5 GeV CEBAF beam. The intensity of the electron beam is limited by the beam dump capacity so a high flux of $\vec{\gamma}$'s necessitates the use high intensity laser light. This high intensity will be achieved by storing the output of a 10 W laser in a Fabry-Perot resonant cavity with a gain of 30,000 and then colliding the electron beam with the stored light. A flux of about 0.2×10^6 $\vec{\gamma}$'s/s/MeV is expected for γ energies of about 600 MeV.

This source has several features which make it ideal for the proposed measurements. First, the two-body kinematics of the Compton process strictly limit the energy of $\vec{\gamma}$'s produced by the backscattering of E_{laser} = 2.4 eV photons from electrons with an energy of E_e = 4.5 GeV to be less than 650 MeV. Unlike the case with bremsstrahlung beams there will be no flux of untagged higher energy γ's. Moreover, the two-body character of the kinematics also dictates that there be a fixed relationship between $\vec{\gamma}$ energy and emission angle. A suitably sized collimator will limit the energies of the $\vec{\gamma}$'s on target to be above 300 MeV. In other words, there will be no low energy "tail" in the $\vec{\gamma}$ energy spectrum.

Second, the cross section for the production of $\vec{\gamma}$'s varies by no more than a factor of 2 across the entire E_γ range, peaking at the highest γ energy (E_γ^{max}) and falling as E_γ decreases, while the γ polarization varies smoothly from almost 100% at $E_\gamma = E_\gamma^{max}$ = 650 MeV to about 35% at 300 MeV. As a result, the figure of merit of the $\vec{\gamma}$ beam has its maximum at the highest energies, just where the cross section for the reaction of interest is smallest. Moreover, the entire energy range of interest can be covered in a single run.

Third, both the $\vec{\gamma}$ and the "recoiling" electron emerge within very small cones centred on the electron beam direction. The small divergence of the γ beam means that the transverse size of the beam on target will be very small (about 4 mm) so a narrow target can be used. This means that emitted π^+'s and recoiling ^{3}H's (as well as p's and d's) will pass through a relatively small amount of material before reaching the CLAS. The divergence of the recoiling electron "beam" will be sufficiently small that the focussing properties of the tagging spectrometer will play essentially no role in determining the energy resolution of the $\vec{\gamma}$ beam. Simply detecting the position of the recoiling electron at a distance from the tagger dipole magnet will be sufficient to fix E_γ. The γ energies in which we are interested lie between 300 MeV and 650 MeV so we will have to detect electrons with energies between 3.85 GeV and 4.20 GeV, (or between about 94% and 85% of E_e), respectively. This will require a new, albeit simple, detector for the tagging spectrometer. Calculations using the measured field profile of the tagging spectrometer magnet[18] indicate that with an array of scintillating fibers having a position sensitivity of 1 mm will be adequate to ensure a photon energy resolution of 2 MeV.

Fourth, there will be no material target in the electron beam. The major potential sources of background are (electron) beam-gas bremsstrahlung and scattering/pair production from the beam collimator. The former contributes very little while the latter, while also small to begin with, can be significantly reduced by one collimator followed by a sweep magnet to deflect charged particles produced at the entrance to the collimator and a second collimator to stop those products. Consequently, backgrounds are expected to be extremely low. It should be noted that the beam-gas bremsstrahlung flux scales to first order with the product of electron current and gas pressure in the beam pipe. Based on nominal beam currents and vacuum pressures the luminosity for this process at LEGS is between 1 and 2 orders of magnitude higher than in Hall B; including beam neutralization effects makes the ratio even higher. The $\vec{\gamma}$ flux in Hall B will be at least an order of magnitude higher than at LEGS, so the background to $\vec{\gamma}$ flux ratio in Hall B will be at least 2 to 3 orders of magnitude lower than at LEGS, where it is already almost negligibly small.

The target to be used is the liquid ^{3}He target designed and being constructed by the Saclay group [12]. The target cell is 16.3 cm long, is nominally 4.3 cm in diameter, and is constructed of 170 μm mylar foil. Because of the very small size of the $\vec{\gamma}$ beam the diameter will be reduced to between 1 cm and 2 cm. While we believe a diameter of 1 cm can be used, we have assumed the

conservative value of 2 cm when simulating the experiment.

The CLAS detector will be used in this measurement. Its features include large acceptance, charged particle tracking and momentum mapping, and particle identification by TOF and dE/dx determination. It covers almost all of the kinematic region containing the physics which this experiment is intended to explore. The trigger for this experiment will consist of a coincidence between the tagging spectrometer and a start counter placed around the target. This start counter is composed of six pieces of plastic scintillator each 3 mm thick [15]. Figure 6 shows a typical event for $E_\gamma = 500 MeV$ and $\theta_\pi = 120°$. In this particular event, both the backward pion (labeled as track 1) and the forward recoiling ^{3}H (labeled as track 2) are detected in coincidence.

The π^+ will be detected by the start counter and then will be tracked by the three regions of drift chambers, where its momentum and the sign of its charge will be determined. Finally, it will be detected by the TOF counter. In general, it will not be possible to detect the recoiling ^{3}H, but when the photon energy is above 400 MeV, some higher energy ^{3}H's ($E_K >$ 50 MeV) can make it through to the TOF counter thereby being identified and momentum analyzed. Other particles (π^-, π^0, p, and d) emerging from other reactions also will be identified and measured. These will be useful in identifying and rejecting background events and will permit us to address auxiliary physics issues connected to the several accessible breakup channels (see Sec. 3.7).

3.2 Resolution

Over most of the kinematic range, identification of the desired reaction channel will rely solely upon the detection of a single π^+. The missing mass associated with the undetected recoiling nucleons will determine whether the reaction that produced the π^+ was an iso-elastic or inelastic process. The thresholds for two-body and three-body disintegration of ^{3}He are 6.78 MeV and 8.48 MeV, respectively, so a missing mass resolution of about 5 MeV is required. For photon energies from 300 MeV to 650 MeV, the resultant pion momenta range from 220 MeV/c to 630 MeV/c. At these momenta the CLAS is expected to have momentum resolution better than 1.0% (FWHM) so with a photon energy resolution of 2 MeV the missing mass resolution will be better than 5 MeV.

In modeling the experiment to obtain a better determination of the missing mass resolution, the following assumptions were made: the energy distribution of the photons has an gaussian shape with an FWHM of 2 MeV; the azimuthal angle ϕ in laboratory system of the charged pion was fixed at 15° and the pion momentum is fixed by the elastic kinematics; the liquid target is contained in a 2 cm diameter and 16.3 cm long mylar cell; a layer of 1 mm carbon fiber beam pipe and the 3 mm start counter (plastic scintillator) surround the target; the diameter of the photon beam is 4 mm. The SDA code [16] was used for the Monte Carlo simulation. The two-body break up events were generated separately using the model described in [17]. The model assumes a quasi-free photon absorption process on a proton in the target nucleus. Accordingly, the cross section has the same general features as that for π^+ photoproduction on a free nucleon but is shifted and spread by the binding energy and Fermi motion in ^{3}He.

Typical spectra for elastic events at 90° produced by 450 MeV photons are shown in figure 10. The spectra from the top to bottom show the broadening in momentum, polar angle, and azimuthal angle, respectively. The momentum resolution is 1.6%, the polar angle resolution is 0.3°, and the azimuthal angle resolution is 0.4°.

Figure 11 shows a pion momentum spectrum at 40.6° for 338 MeV photons. A clear separation of the elastic peak and the broad quasi-free peak can be seen. As a comparison, the spectrum at the same energy and angle from the Saclay data of d'Hose *et al.* [17] is shown in figure 12.

Figure 13 and 14 shows momentum spectra for two energies and three angles. Figure 15 shows the missing mass spectrum for 450 MeV photons at 90°.

From these Monte Carlo simulations it is seen that the resolution is easily adequate to separate the elastic peak from two-body and three-body break up processes. In the experiment, it will be necessary to group the data into bins in the polar angle θ_π of at least 1° in width. The effect of this binning on our ability to separate elastic from inelastic channels depends upon the dependence of pion momentum on pion angle. This dependence is shown in figure 16 where, in most cases, the derivative of the momentum to angle is less than 1 MeV/°. Polar angle bin widths of a few degrees will be possible.

3.3 Acceptance

In order to evaluate the solid angle acceptance of the CLAS for this reaction elastic events corresponding to 450 MeV $\vec{\gamma}$'s were generated and distributed uniformly over a polar angle range from 10° to 140°. Figure 17 shows the CLAS acceptance as a function of pion polar angle θ_π. As expected, the acceptance has a cut off at both forward (10°) and backward (120°) angles. With photon energies between 300 MeV and 650 MeV this angular coverage corresponds to a Q^2 range from 0.08 fm^{-2} to 20 fm^{-2}.

Figure 18 shows the acceptance as a function of the azimuthal angle ϕ. The ϕ acceptance extracted from this simulation is about 70%. Moreover, it has a rather complicated functional dependence. Uncertainties associated with this dependence will be minimized in this experiment by varying randomly and often the orientation of the $\vec{\gamma}$ polarization vector.

Figure 19 illustrates the ^{3}H acceptance as a function of the momentum of the recoiling ^{3}H. The upper graph shows the initial spectrum, while the bottom shows the spectrum of those reaching the TOF counter (in coincidence with a π^+ reaching the TOF counter). The large shift in the spectrum is due to the large dE/dx of this heavier nucleus. For an incident $\vec{\gamma}$ energy of 450 MeV, 30% of the recoiling ^{3}H's can be detected. The sharp discontinuity in the energy of ^{3}H's reaching the TOF detector is due to the presence of a sharp corner in the vertex detector. Figure 20 shows the Q^2 dependence on angles for different photon energy in c.m. system.

3.4 Recoil Detection

As described earlier, the principal particle to be detected is the charged pion. When the π^+ is emitted in the forward direction the kinetic energy of the recoiling ^{3}H is too low to be detected. However, when the π^+ is emitted at backward angles it will be possible to detect the recoiling ^{3}H. The main problem in detecting the recoiling ^{3}H is its larger energy loss which will prevent it from reaching the TOF counter.

Table 1 lists all the material and their distances from the target center as well as the thickness and the density of each layer inside CLAS[19]. Table 2 lists the energy evolution through these material for an initial ^{3}H kinetic energy of 100 MeV; and Table 3 lists the same for an initial ^{3}H kinetic energy of 50 MeV. ΔE is the energy loss in each layer and E_{res} is the residual

energy after each layer. Generally speaking, the threshold energy for a ^{3}H to be detected by CLAS is about 50 MeV, corresponding to a momentum of 532 MeV/c. Figure 21 shows the dependence of the ^{3}H kinetic energy on the π^+ emission angle for different $\vec{\gamma}$ energies. In order to detect a significant number of ^{3}H's, the $\vec{\gamma}$ energy must be greater than 400 MeV.

The principal advantage to be gained by the detection of a recoiling nuclear product will be the suppression of backgrounds, especially when the $\vec{\gamma}$ energy is highest and the cross section is the smallest. For example, figure 22 shows the tight correlation between the azimuthal emission angles of the π^+ (ϕ_π) and the ^{3}H (ϕ_{recoil}). In addition, when the missing mass as determined by the $\vec{\gamma}$ energy and the π^+ kinematics is close to the mass of the ^{3}H the detection (or not) of a recoiling p or d will indicate whether the event was or was not from elastic process.

3.5 Event Rate and Trigger

The time required to obtain a good measurement of the asymmetries can be estimated starting from the cross section and asymmetry at 90° in the c.m. frame as shown in figure 7. A photon flux of about 0.2×10^6 MeV^{-1}sec^{-1} was assumed with the flux at each energy taken from figure 8 in [11]. The target was assumed to be liquid ^3He 16.3 cm long with a density of 64 mg/cm^3. A $\vec{\gamma}$ energy bin of 10 MeV was assumed. For incident photons in the energy range from 300 MeV to 500 MeV, θ_π= 90° in the c.m. frame corresponds approximately to 82° in the laboratory frame. A 5° θ_π bin covering from 79.5° to 84.5° was similarly assumed. Factoring in the 70% acceptance in ϕ_π, the effective π^+ solid angle subtended was 0.38 sr.

The projected counting rates are presented in table 4. Since we are interesting in the photon asymmetry, the events parallel and perpendicular to the reaction plane must be separated. Let $N^\perp$ and $N^\parallel$ represent the total event number perpendicular and parallel to the reaction plane, $N^\perp \propto d\sigma/d\Omega^\perp$ and $N^\parallel \propto d\sigma/d\Omega^\parallel$, and we have

$$\Sigma = \frac{N^\perp - N^\parallel}{N^\perp + N^\parallel}$$

The statistical uncertainty is then given by

$$\Delta\Sigma = \sqrt{\frac{4N^{\perp}N^{\parallel}}{(N^{\perp}+N^{\parallel})^3}}.$$

The estimated precision is shown in table 4 and is shown by the error bars on the points in figure 7.

The anticipated precision of the data is adequate, but not excessive, to examine the various contributions. Based on these estimates, we are requesting 300 hours of beam time.

In addition to the events in the iso-elastic channel of pion photoproduction, there will be a large number of events corresponding to other channels, as well as background from the endcaps of the liquid target cell. The combination of the real event rates from all possible sources is limited by the acceptance of the CLAS data acquisition system.

In estimating the total event rate from the target, the target is taken to be 16 cm long with a density of 0.064 g/cm^2, the photon flux about $5 \times 10^7/sec$, and the total photon absorption cross section about 180 μb/nucleon. This gives a total event rate from the target of about 5kHz. The thickness of the mylar endcaps of the target cell is $170\mu m$ with a density 1.39 g/cm^2, so the total event rate will be about 250Hz, or about 5% of the total rate.

The CLAS design calls for a four level trigger system. We will set up a data selection criteria at each level. Before the event is sent to trigger level one, a preselection will be made using the start counters. Since there are only two charged particles in the final state, we will select those events which have either one hit or two hits in a pair of opposing sectors of the start counter. The preselection will eliminate about 2/3 of the events containing multiple charged particles generated, for example, by two- and three-body disintegration. Hence, we will have an event rate of about 1.7 kHz rate entering the CLAS trigger system. At level one, a trigger is formed by information from the TOF, Cerenkov, and calorimeter detectors. This trigger level is expected to have a processing time of 200 nsec so the expected event rate is well within the capability of the system. Since we are looking for events with only charged particles in the final state, any detection of a neutral particle in the calorimeter will cause the event to be rejected. This will eliminate at least 50% of the surviving events. Accordingly, after trigger level one the event rate will be reduced to less than 1 kHz.

At level two, crude tracking will be performed using the drift chambers to determine if the hits in the TOF detector and calorimeter are due to charged particles or to the conversion of a neutral particle. Neutral particles and events with more than two hits will be eliminated. The time required at level two is 2 μsec so again the projected rate is well within the capability of the system.

Level three forms track segments from the hits in the drift chambers to get crude measurements of momenta and angles. First, events containing negatively charged particles will be rejected. If there are two surviving tracks, only those events where the tracks in opposite sectors lie within a 5° azimuthal angular range will be kept. This will suppress the rate by another order of magnitude, leaving a rate of 100 Hz reaching level 4. Level three will take about 1-20 μsec.

At level four, each event will be fully reconstructed. Proton and deuteron tracks can be recognized from TOF spectra and will be rejected. Thus, two- or three-body disintegration events can be completely suppressed. With the information on the vertex position, events originating in the endcaps will be rejected. After these cuts, it is expected that the event rate will be below 10 Hz. This event rate should pose no problems for the data acquisition system. In actuality, it is very possible that we willbe able to loosen the criteria to have a wider range of events accepted. This would enable us to acquire data on reactions that until now have been regarded as background.

3.6 Systematic Errors

The lifetime of the π^+ is 26 nsec and the corresponding value of $c\tau$ is 780 cm, comparable to the distance from the target to the last detector. For example, the velocity of a π^+ with 300 MeV of kinetic energy is 0.95 c. Its lifetime in the laboratory frame is

$$T_{lab} = T_{cm}/\sqrt{(1-\beta^2)} = 83ns$$

For a representative flight path of 3.5 m, the time of flight is 12 nsec. Therefore, the probability of surviving after this distance is 86%. Corrections for pion decay will be required in the data processing; muons emerging from the decay of π^+'s can be distinguished by the dE/dx versus momentum distribution in the TOF counter.

Another possible loss mechanism is through nuclear interactions in the detector material. The thickest pieces are the start and TOF counters. Although the TOF counter is 5 cm thick, it does not matter whether the π^+ interacts with a nucleus there or not, just so long as enough energy (2.5 MeV) is deposited in the detector to produce a signal for TOF. For the 3mm thick plastic scintillator of the start counter, we can estimate the fraction of π^+'s that will be lost by noting that a pion-nuclear total cross section is of the order of 40 millibarns. The macroscopic total cross section (or reaction probability per unit length) is about 2×10^{-3} cm^{-1} and the probability of absorption will be about 6×10^{-4}. Accordingly, this effect can be neglected in this measurement.

3.7 Additional Accessible Physics

In addition to the reaction $^3He(\vec{\gamma},\pi^+)^3H$, data on several other reactions will simultaneously be available:

$$^3He(\vec{\gamma},\pi^+)nd$$
$$^3He(\vec{\gamma},\pi^+n)d$$
$$^3He(\vec{\gamma},\pi^+n)pn$$
$$^3He(\vec{\gamma},\pi^+d)n$$
$$^3He(\vec{\gamma},\pi^+nd)$$

$$^3He(\vec{\gamma},\pi^-)ppp$$

$$^3He(\vec{\gamma},p)d$$
$$^3He(\vec{\gamma},d)p$$
$$^3He(\vec{\gamma},p)pn$$

$$etc.$$

First, there are the two-body and three-body break up channels, where meson-exchange currents and possibly off-shell operator effects may play roles [5].

In addition, there is the the conjugate process, π^- photoproduction. Unlike the π^+ case, no elastic peak in the momentum spectrum can exist. In addition to their intrinsic interest, these data could be useful in fixing the location of the quasi-free peak and could help us to estimate the contributions of the break up channels.

Unfortunately, coherent or elastic π^0 photoproduction will be difficult to measure with any precision. The recoiling ^{3}He's will have energies too low to be detected in the CLAS. The electromagnetic shower counter will be able to detect the two π^0 decay photons but the missing mass resolution is expected to be about 40 MeV, inadequate to isolate elastic events from the two- and three-body photodisintegration channels.

The two-body photodisintegration of ^{3}He has been studied both experimentally and theoretically [20] at lower photon energies. It was found that the meson exchange contribution is very important and that the cross section is very sensitive to the details of the nuclear model. The fit to the data is significantly improved when d-wave components are added to the wave functions of the spectator nucleon and/or deuteron. The currently proposed experiment could extend this study to higher energies.

The three-body photodisintegration of ^{3}He has been studied experimentally at Saclay [21]. It was predicted that three-nucleon absorption would play a significant role in the momentum region between the quasi-free and the $^3He(\gamma, p)d$ peaks where the cross section was systematically underestimated by calculation. The experimental data were largely limited by bremsstrahlung contamination in producing the γ beam. The proposed Compton $\vec{\gamma}$ source will not have this problem and the higher quality data may make it possible to clarify this ambiguity.

3.8 Related Experiments

There are two approved experiments in Hall B on photon induced reactions on ^{3}He: PR 93-044 and PR 91-014. There is no overlap between the experiment proposed here and these two proposals. First, the two currently approved experiments will use only unpolarized photons; no polarized observables will be measured. Second, they plan to run at significantly higher energies, $E_\gamma > 500 MeV$. The Compton $\vec{\gamma}$ source (in its initial configuration with $\lambda_{laser} =$ 514 nm and an electron energy of 4.5 GeV) has a sharp cut off at 650 MeV. Finally, the physics foci of these experiments, strange production and multi-

pion production, are very different from that of the experiment proposed here.

3.9 Choice of Facility

The proposed experiment requires the unique combination of capabilities offered by the CLAS detector and the Compton $\vec{\gamma}$ source proposed for Hall B. The cross sections are small and measurements over a wide range of pion production angles are required so the broad acceptance of the CLAS is crucial. It is necessary to identify iso-elastic events by reconstructing the missing mass accurately so the relatively high precision of the CLAS detector is required. The small cross sections also necessitate the high flux of highly polarized photons that the Compton $\vec{\gamma}$ source will provide. Finally, the simplicity of the final state of prime interest (^{3}H + π^+), of which only the π^+ usually will be detected, requires that background levels be kept very low. The quality of the measurements will be enhanced by the low systematic uncertainties resulting from the ease with which the photon polarization can be arbitrarily rotated, the high precision to which the polarization is known, and the fact that the entire γ energy range can be covered in one run.

Few other sources of linearly polarized photons either currently exist or are planned[23]; none are suitable for this measurement.

- LEGS: The maximum photon energy at LEGS will be approximately 480 MeV when the frequency doubled laser is used, insufficient for this experiment. In addition, the energy resolution of the γ beam is about 5.5 MeV. Unless the iso-elastic channel is identified by detecting the recoiling ^{3}H this resolution, coupled with the low resolution of existing detectors at LEGS, is inadequate. The idea of performing the experiment at LEGS using recoil detection was evaluated but it was determined that the combination of low γ flux and thin target required to allow the ^{3}H's to escape resulted in prohibitively low counting rates.

- GRAAL: The maximum γ energy at GRAAL will be about 1.1 GeV but the energy resolution will be even worse than at LEGS, about 15-20 MeV. The flux will be comparable to that at LEGS so attempting the measurement using ^{3}H detection would suffer from the same prohibitively low rates.

- Spring-8: The planned energy resolution is about 20 MeV with fluxes comparable to those of LEGS at GRAAL.

- TUNL/DFELL: The maximum energy of this proposed facility is about 200 MeV.

- Mainz: The maximum electron energy at Mainz is about 850 MeV and linearly polarized photons are produced by coherent bremsstrahlung from a diamond. The polarization of γ 's with energies above 500 MeV (where the small cross sections make a high figure of merit imperative) produced by an 850 MeV beam are much too low to be useful for the proposed experiment.

- Bonn: The γ energy resolution is 10 MeV and the flux is comparable to LEGS. Accordingly, the need for recoil detection at all kinematics would necessitate the same thin targets and the same prohibitive event rates as at LEGS.

- CEBAF-Coherent Bremsstrahlung: The other $\vec{\gamma}$ source proposed for Hall B[22] promises polarization at higher photon energies when the electron beam is limited to 6 GeV than does the Compton $\vec{\gamma}$ source. However, its figure of merit[11]

$$\mathcal{F}_m = N_\gamma < P_\gamma^2 > \eta,$$

is much lower *for this measurement.* Here, N_γ is the γ flux per MeV, P_γ is the average photon polarization, and η is the tagging efficiency. While the various parameters are flexible, polarization can be increased at the expense of energy range and tagging efficiency, optimal polarization with bremsstrahlung sources occurs for photons with energies approximately $\frac{1}{3}$ of the electron energy. Based upon results from Mainz, currently the best coherent bremsstrahlung facility in operation, one can expect an average γ polarization of not more than 50-70% over a range of γ energies of about 10% of the electron beam energy and a tagging efficiency of about 50%. Significantly, about 90% of the γ beam is unpolarized. The projected maximum total tagging rate is about 5×10^7/s so two operating scenarios are possible. First, one could operate the entire tagger detector and accept an effective N_γ for the polarized portion of about 5×10^6/s. This would yield a figure of merit $\mathcal{F}_m$ a factor of 40-80 lower

than that obtainable with the Compton source. Since the beam has a 5×10^8 Hz structure a final resolving time of 2 ns would be adequate to limit the average multiplicity to very close to 1 just as with the Compton source. The alternative is to activate only those channels corresponding to photons with energies in the range where there is significant polarization. Increasing the rate in these channels to the limit of 5×10^7/s would bring the figure of merit to within a factor of 2-4 of the Compton source, but at the expense of having a flux of untagged photons of almost 5×10^8/s. This rate, which closely matches the microstructure of the electron beam, would result in an average multiplicity *after all possible timing cuts are made* approaching 2. For most of the kinematic range of interest we detect only one reaction product (π^+) so vertex reconstruction cannot help to reduce the final multiplicity. At all energies of interest here but particularly at the higher energies the ^{3}He$(\vec{\gamma}, \pi^+)$ cross section is dominated by quasi-free production. Accordingly, the missing mass spectrum generated by the accidental coincidences would be smooth and large. For events corresponding to γ 's with energies above about 400 MeV this background would completely obscure the iso-elastic peak.

The above considerations do not take into account either the higher levels of background radiation or the flux of high energy, untagged photons that inevitably accompany a bremsstrahlung beam. In view of the simplicity of the final state (usually one detected π^+) these backgrounds would generate a disproportionate contribution to the spectrum. Finally, it must be noted that the smooth and extremely well understood energy dependence of the Compton scattering cross section and photon polarization as well as the ease and rapidity with which the polarization of the beam can be rotated through arbitrary angles reduces the level of systematic uncertainties relative to those associated with a coherent bremsstrahlung source.

In sum, the unique combination of the CLAS detector and the proposed Compton $\vec{\gamma}$ source constitute the only facility at which the proposed measurement can be performed within a reasonable amount of time.

4 Summary

We are requesting 300 hours beam time for the measurement of photon cross sections and asymmetries for the reaction $^3He(\vec{\gamma},\pi^+)^3H$. The broad kinematic range to be spanned by the data will enable us to access a rich body of physics related to the interaction of photons and pions with nuclei and, most importantly, possible modifications of the properties of the Δ in a dense nuclear system. The measurements require the unique combination of capabilities promised by the CLAS detector and the proposed Compton $\vec{\gamma}$ source; they cannot be performed at any other existing or planned facility.

References

[1] S.S. Kamalov, L. Tiator, and C. Bennhold, Nucl. Phys. A547(1992)599.

[2] J.R. O'Fallon, L.J. Koester, Jr., J.H. Smith, and A.I. Yavin, Phys. Rev., 141(1966)889.

[3] D. Bachelier, M. Bernas, J.L. Boyard, J.C. Jourdain, P. Radvanyi, Phys. Lett. B 44(1973)44; Nucl. Phys. A251(1970)433.

[4] S.S. Kamalov, L. Tiator, and C. Bennhold, Phys. Rev. Lett. 75(1995)1288.

[5] N. d'Hose, G. Audit, A. Bloch, N. de Botton, L. Ghedira, L. Jammes, J.M. Laget, J. Martin, E. Mazzucatto, C. Schuhl, G. Tamas, E. Vincent, M. Rodgers, P. Stoler, P. Argen, A. Braghieri, and P.Pedroni, Nucl. Phys. A554(1993)679.

[6] B. Bellinghausen, H.J. Gassen, G. Nöldeke, E. Reese, T. Reichelt, P. Stipp, and H.A. Synal, Nucl. Phys. A470(1987)429.

[7] L. Tiator, A.K. Rej and D. Drechsel, Nucl. Phys. A333(1980)343; J.L. Ballot, C. Lazard and Z. Maric, Nucl. Phys. A395(1983)471.

[8] S.S. Kamalov, L. Tiator, and C. Bennhold, Few-Body Systems, 10(1991)143.

[9] J. M. Laget, Nucl. Phys. A481(1988)765.

[10] R. A. Miskimen *et al.*, CEBAF Proposal PR-94-015.

[11] B. E. Norum, and P. Welch, LOI, April 1993.

[12] C. Marchand, Private communication.

[13] C. Bennhold, Private communication.

[14] J.M. Koch, and E.J. Moniz, Phys. Rev. C27(1983)751.

[15] G. Mutchler, private communication.

[16] Bogdan Niczyporuk, private communication.

[17] N. d'Hose, thesis, 1988, Saclay.

[18] Dan Sober, private communication.

[19] Elton Smith, private communication.

[20] J. M. Laget, in 'New Vistas in Electro-nuclear Physics', P361, Ed. by E.L. Tomusiak, *et al.*, Plenum Press, 1985.

[21] N. d'Hose, G. Audit, A. Bloch, N. de Botton, L. Ghedira, L. Jammes, J.M. Laget, J. Martin, E. Mazzucatto, C. Schuhl, G. Tamas, E. Vincent, M. Rodgers, P. Stoler, P. Argen, A. Braghieri, and P.Pedroni, Phys. Rev. Lett., 63(1989)856.

[22] B. Berman, private communication, 1994.

[23] B. E. Norum, in 'Spin Degrees of Freedom in Electromagnetic Nuclear Physics', P123, Ed. by V. Burkert, Oct. 1994.

[24] N. Bianchi *et al.*, Phys. Lett. **B309** (1993) 5.

Table 1: Material for a particle to travel through in CLAS.

layer	item	material	dist. cm	thick. cm	density g/cm^3
1	target	L^3He	2.0	2.0	0.064
2	cell	mylar	2.0	0.017	1.39
3	pipe	C-fiber	70	0.1	1.65
4	space	Helium	85	15	1.78×10^{-4}
5	trig.	scint.	85	0.3	1.032
6	space	Helium	100	15	1.78×10^{-4}
7	reg. 1	mylar	100	0.005	1.39
8	reg. 1	Ar-CH4	115	15	1.57×10^{-3}
9	reg. 1	mylar	115	0.005	1.39
10	space	Helium	155	40	1.78×10^{-4}
11	reg. 2	mylar	155	0.005	1.39
12	reg. 2	Ar-CH4	185	30	1.57×10^{-3}
13	reg. 2	mylar	185	0.005	1.39
14	space	Helium	250	65	1.78×10^{-4}
15	reg. 3	mylar	250	0.005	1.39
16	reg. 3	Ar-CH4	310	60	1.57×10^{-3}
17	reg. 3	mylar	310	0.005	1.39
18	TOF	scint.	500	5	1.032

Table 2: Energy evolution of 100 MeV ^3H in CLAS

layer	material	dE/dX MeV/cm	Δ E MeV	E_{res} MeV	TOF nsec
1	L^3He	1.51	3.26	96.7	0.26
2	mylar	21.8	0.37	96.4	0.26
3	C-fiber	25.4	2.54	93.8	9.25
4	Helium	0033	0.05	93.8	11.2
5	scint.	17.3	5.2	88.6	11.2
6	Helium	0.0035	0.05	88.6	13.3
7	mylar	23.3	0.12	88.4	13.3
8	Ar-CH4	0.027	0.44	88.0	15.3
9	mylar	23.5	0.12	87.9	15.3
10	Helium	0.0035	0.14	87.7	20.8
11	mylar	23.51	0.12	87.6	20.8
12	Ar-CH4	0.028	0.83	86.8	24.9
13	mylar	23.7	0.12	86.7	24.9
14	Helium	0.0035	0.23	86.5	33.8
15	mylar	23.8	0.12	86.3	33.8
16	Ar-CH4	0.028	1.68	84.7	42.2
17	mylar	24.2	0.12	84.5	42.2

Table 3: Energy evolution of 50 MeV ^3H in CLAS

layer	material	dE/dX MeV/cm	Δ E MeV	E_{res} MeV	TOF nsec
1	L^3He	2.80	6.03	43.8	0.38
2	mylar	41.4	0.70	43.3	0.38
3	C-fiber	50.7	5.07	38.2	14.4
4	Helium	0.007	0.11	38.1	17.3
5	scint.	40.5	12.1	25.9	17.3
6	Helium	0.010	0.15	25.8	21.0
7	mylar	63.6	0.32	25.5	21.0
8	Ar-CH4	0.077	1.23	24.3	24.9
9	mylar	66.9	0.33	23.9	24.9
10	Helium	0.01	0.41	23.5	35.2
11	mylar	68.6	0.34	23.2	35.2
12	Ar-CH4	0.085	2.55	20.6	43.5
13	mylar	76.3	0.38	20.2	43.5
14	Helium	0.012	0.78	19.5	62.0
15	mylar	80.0	0.40	19.1	62.0
16	Ar-CH4	0.11	6.67	12.4	83.4
17	mylar	115.5	0.58	11.8	83.4

Table 4: Event rate and precision for $\Theta_{c.m.} = 90^{o}$.

E_{γ} MeV	300	350	400	450	500
$\frac{d\sigma}{d\Omega}\mu b/sr$	1.54	0.17	0.028	0.013	0.07
flux MHz/MeV	0.16	0.17	0.20	0.24	0.29
rate Hz/sr/MeV	0.52	0.0061	0.0012	6.6E-4	4.3E-4
$\Delta\Omega$ sr	0.38	0.38	0.38	0.38	0.38
ΔE MeV	10.0	10.0	10.0	10.0	10.0
rate Hz	0.2	0.023	0.045	0.0025	0.0016
events in 300 hrs	216k	24.9k	4.8k	2.7k	1.7k
Σ	0.43	0.60	0.37	0.11	0.10
$N^{\perp} + N^{\parallel}$	24.3k	2.77k	530	300	190
$N^{\perp} - N^{\parallel}$	10.3k	1.66k	200	30	19
$N^{\perp}$	17.3k	2.21k	365	170	100
$N^{\parallel}$	7.0k	560	170	133	86
$\Delta\Sigma$	0.006	0.015	0.04	0.06	0.07

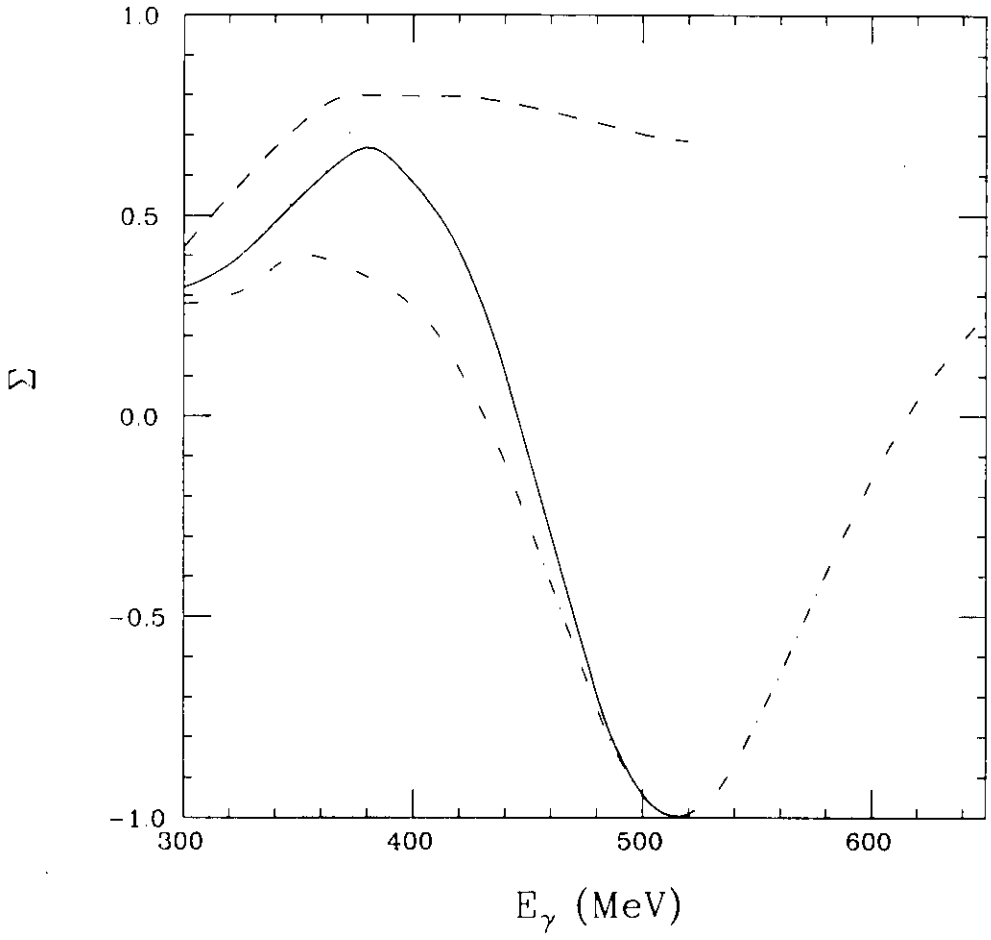

Figure 1. Plane wave results for energy dependence of photon asymmetry at $\theta = 90°$. The solid (dashed) curves are calculated with (without) D-state components of the three-body wave function and the full production operator. The dash-dotted (dotted) curves are calculated without the $E_{1+}(\Delta)$ multipole and with (without) D-state components of the three-body wave function.

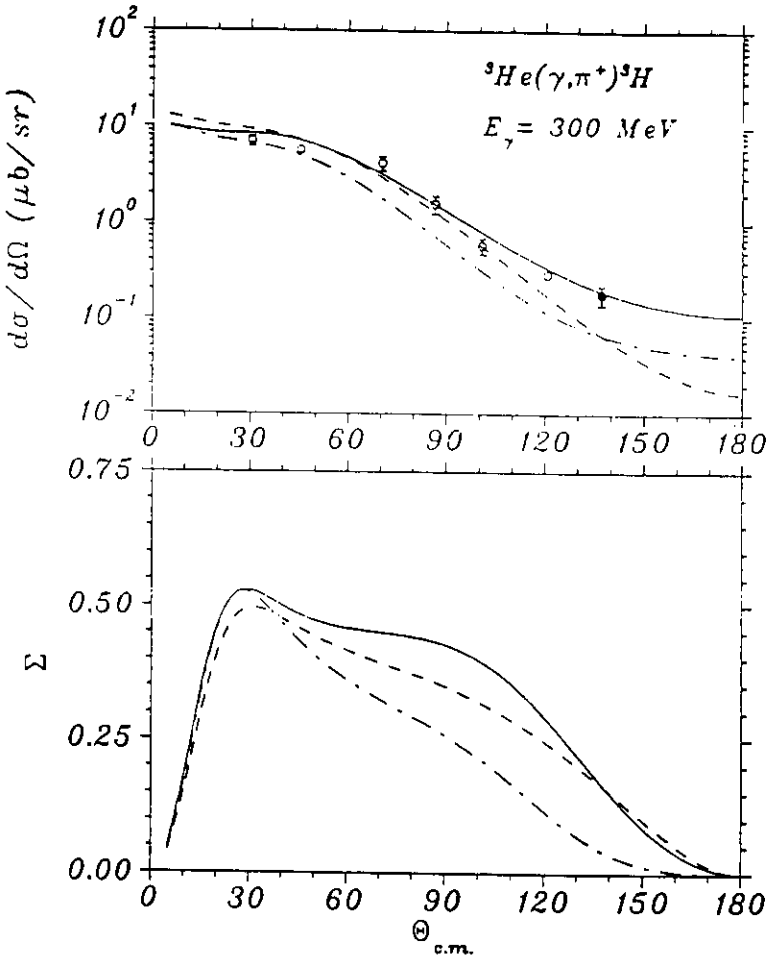

Figure 2. Angular dependence for $d\sigma/d\Omega$ and photon asymmetry at $E_\gamma = 300MeV$, calculated with the full three-body wave function and the full production operator. The solid, dash-dotted, and dashed curves are obtained in the coupled-channels approach that includes two-step processes, in DWIA and PWIA, respectively.

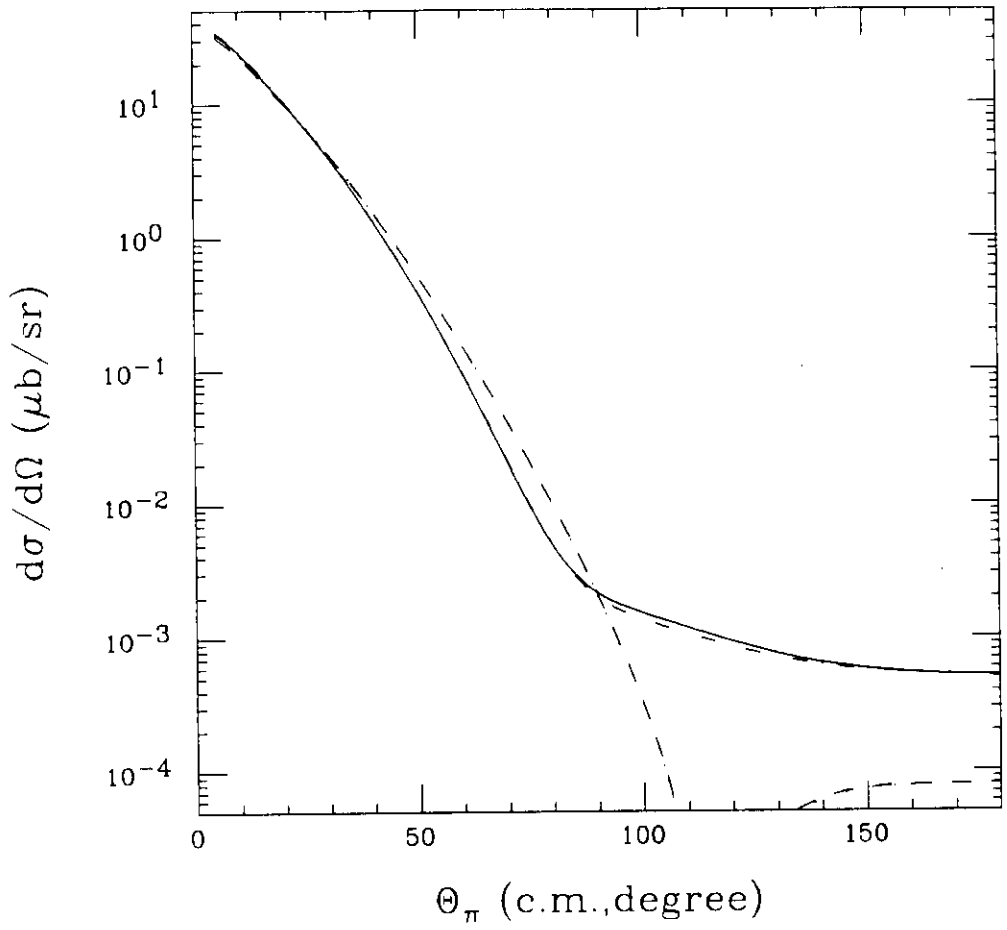

Figure 3. Angular dependence for $d\sigma/d\Omega$ at $E_\gamma = 520 MeV$ from plane wave results, The solid (dashed) curves are calculated with (without) D-state components of the three-body wave function and the full production operator. The dash-dotted (dotted) curves are calculated without the $E_{1+}(\Delta)$ multipole and with (without) D-state components of the three-body wave function.

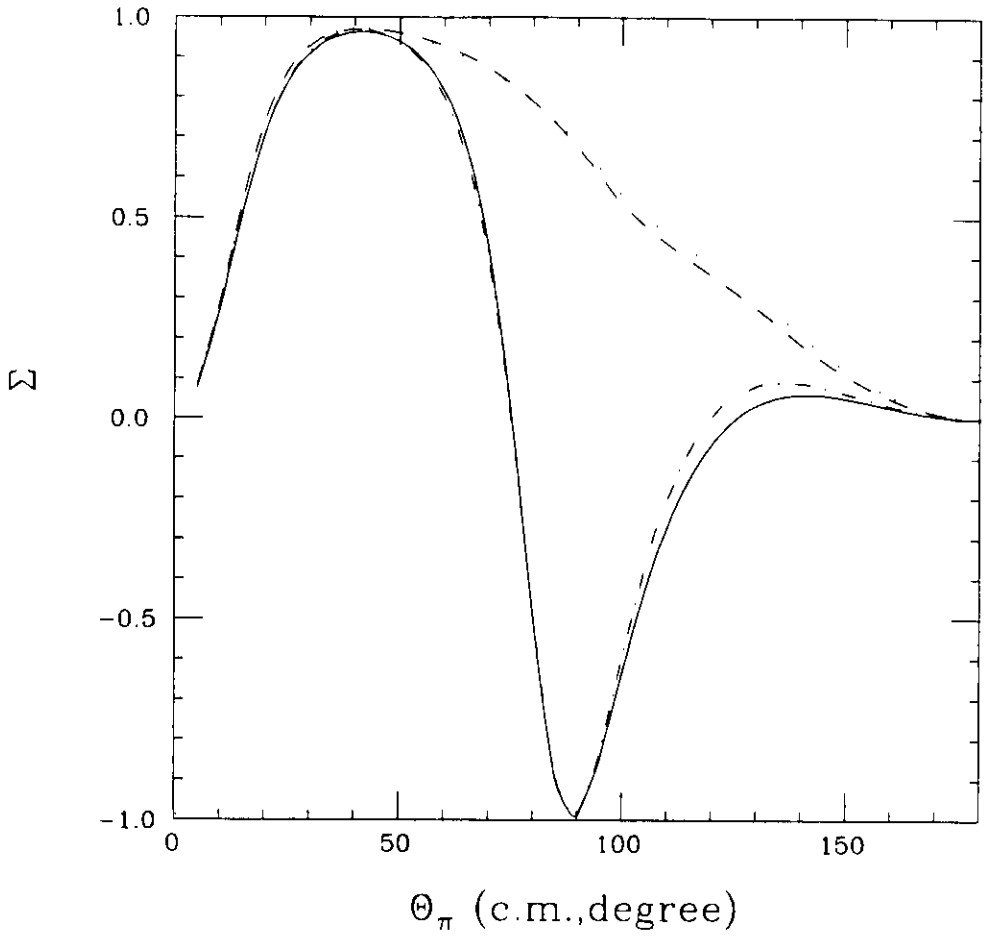

Figure 4. Angular dependence for photon asymmetry at $E_\gamma = 520 MeV$ from plane wave results, calculated with the full three-body wave function and the full production operator. The solid, dash-dotted, and dashed curves are obtained in the coupled-channels approach that includes two-step processes, in DWIA and PWIA, respectively.

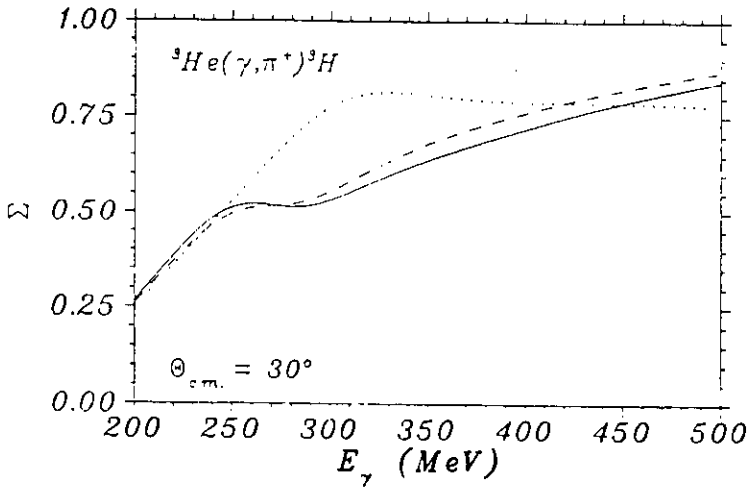

Figure 5. Energy dependence of photon asymmetry at $\theta = 30°$. The solid (dashed) curves are calculated with (without) D-state components of the three-body wave function in the coupled-channels framework and with the full production operator. The dotted curves are calculated without the full three-body wave function but only with Born terms in the production operator.

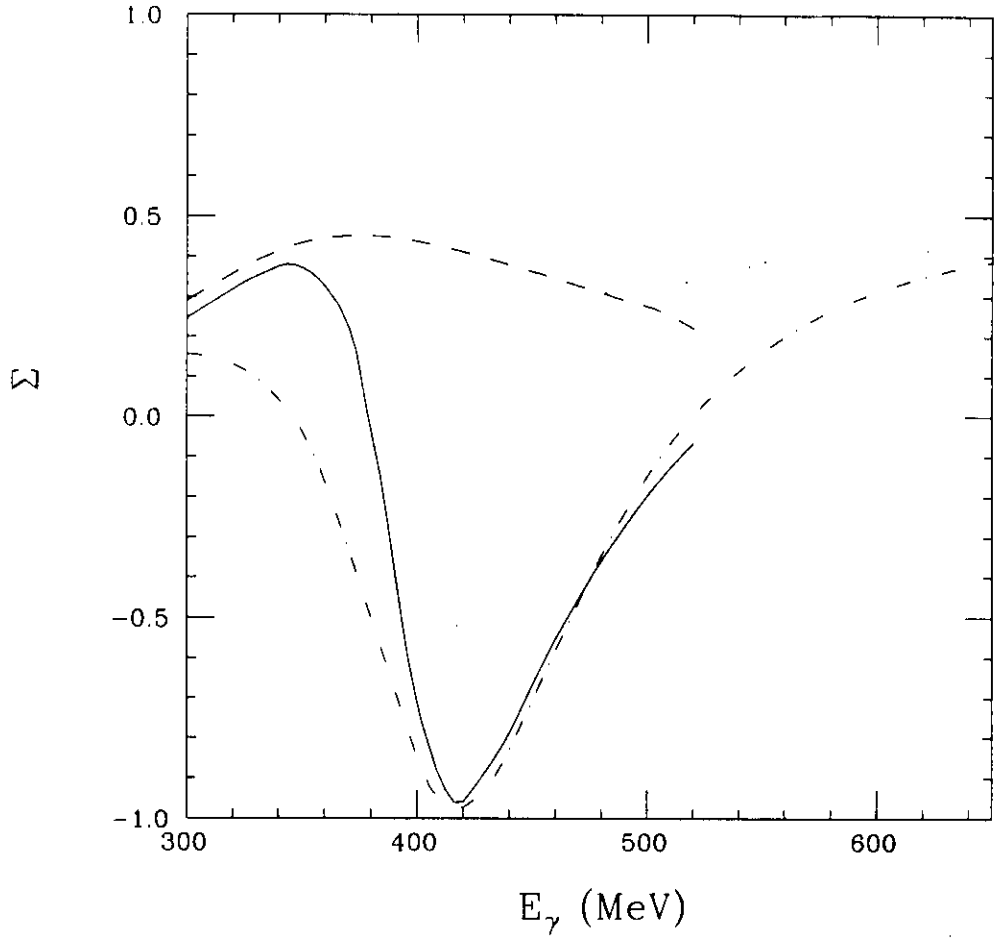

Figure 6. Plane wave results for energy dependence of photon asymmetry at $\theta = 120^{\circ}$. The solid (dashed) curves are calculated with (without) D-state components of the three-body wave function and the full production operator. The dash-dotted (dotted) curves are calculated without the $E_{1+}(\Delta)$ multipole and with (without) D-state components of the three-body wave function.

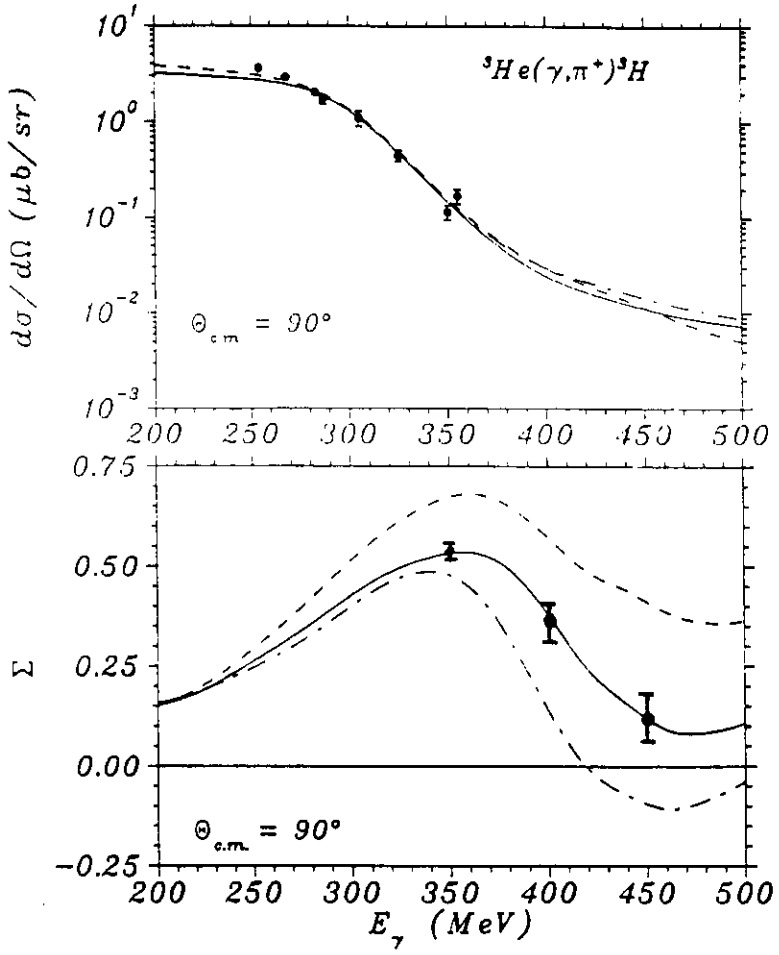

Figure 7. Energy dependence of cross section and photon asymmetry at $\theta = 90°$ calculated in the coupled-channels framework. The solid (dashed) curves are calculated with (without) D-state components of the three-body wave function and the full production operator. The dash-dotted curves are calculated without the $E_{1+}(\Delta)$ multipole but with D-state components of the three-body wave function. The error bars of photon asymmetry are expected from this measurement.

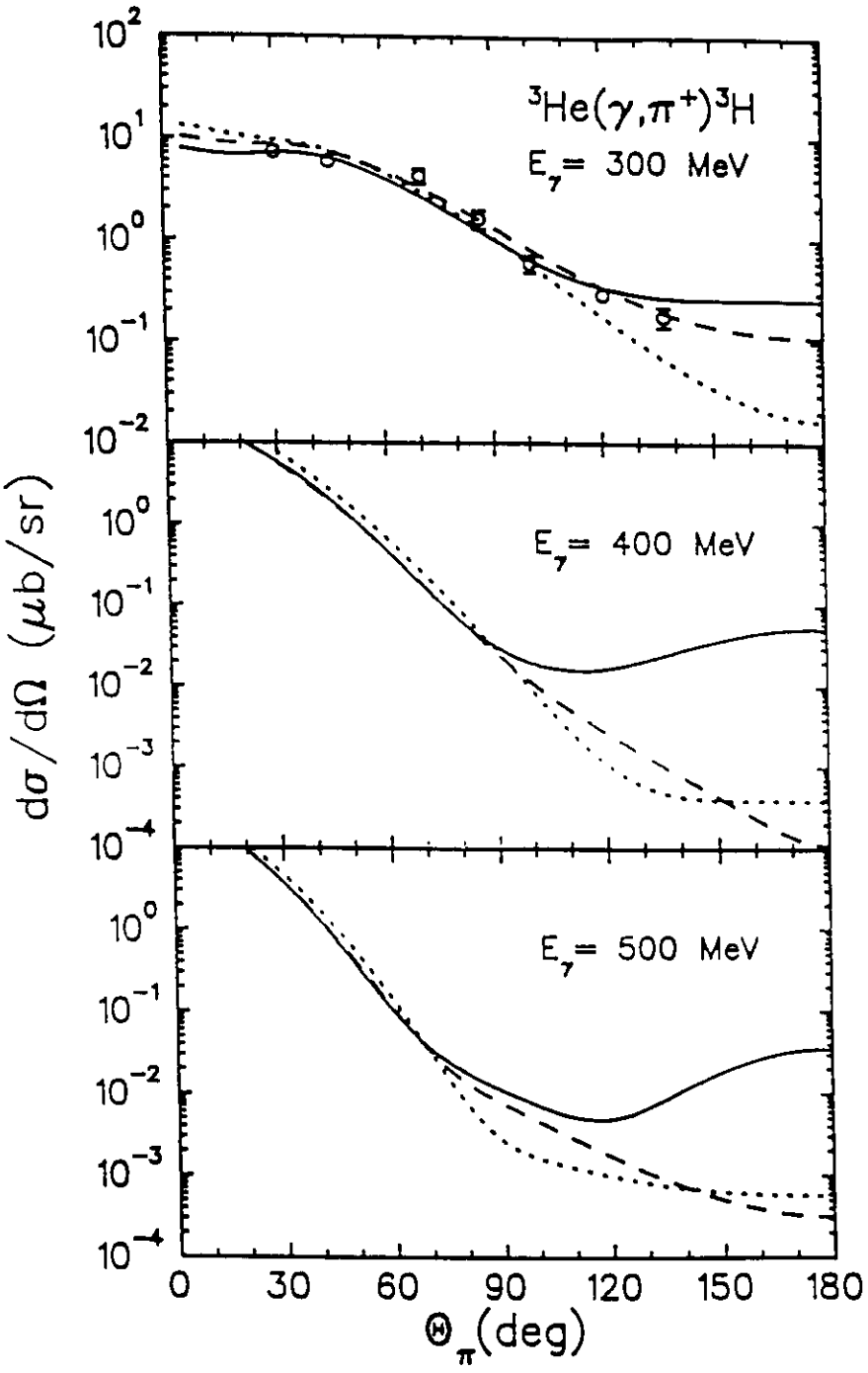

Figure 8. Pion angular distribution for three photon energies. The dotted (dashed) curves show the PWIA (DWIA) results obtained with Faddeev wave functions. The full line shows the KTB complete calculation with the two-body mechanism.

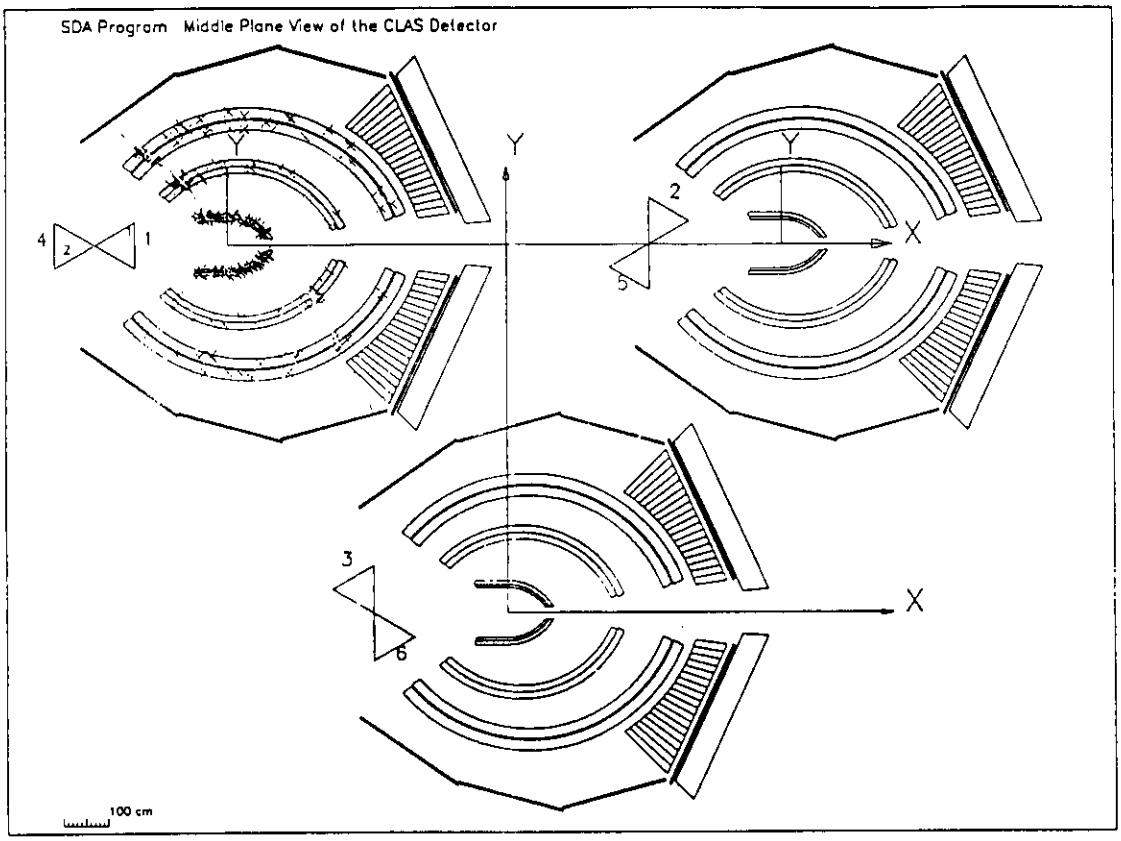

Figure 9. Typical event at CLAS for $E_\gamma = 500MeV$ and $\theta_\pi = 120°$.

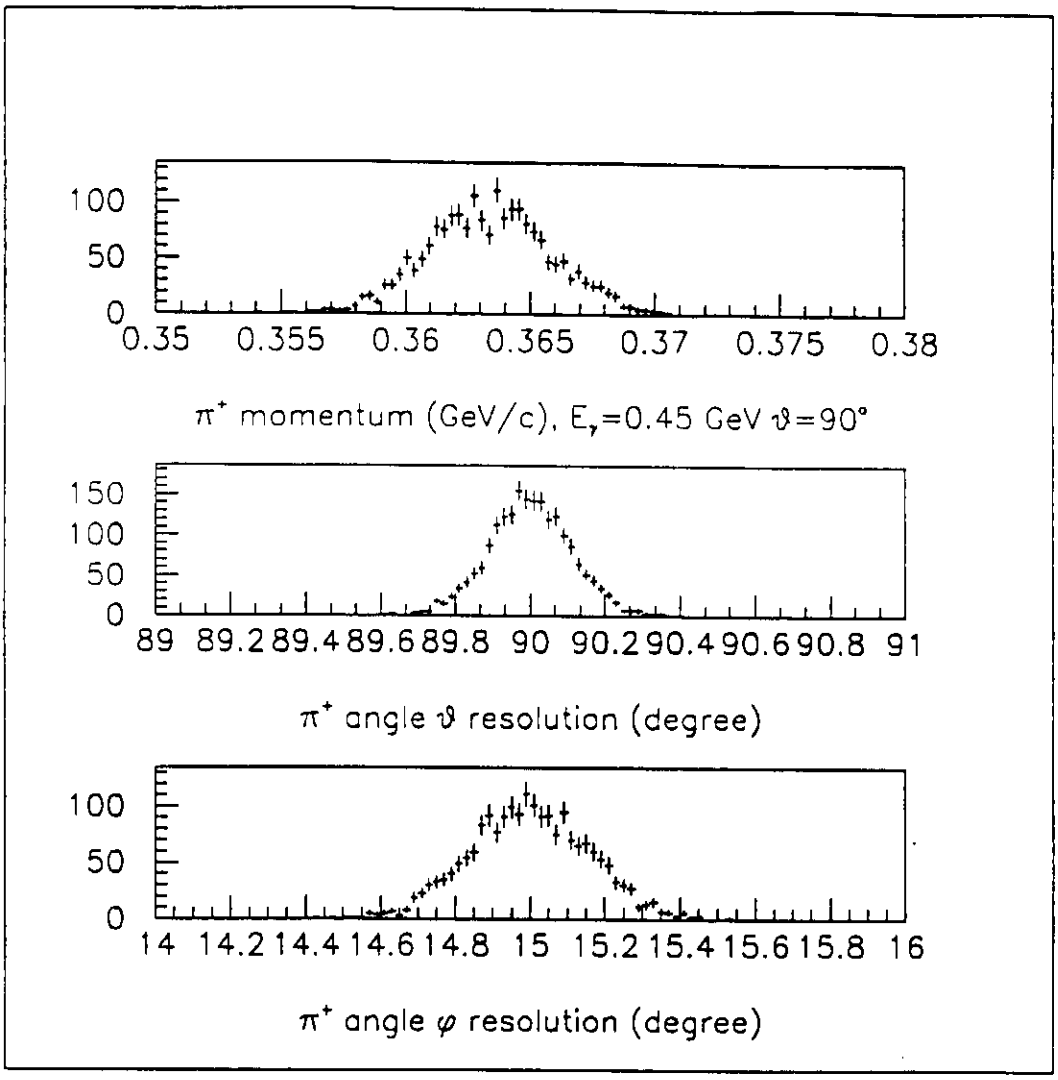

Figure 10. Resolution for pion measurement at $E_\gamma = 450 MeV$ $\theta_\pi = 90°$. The top is the momentum resolution for elastic channel, the middle shows polar angle resolution, and the bottom shows azimuthal angle resolution.

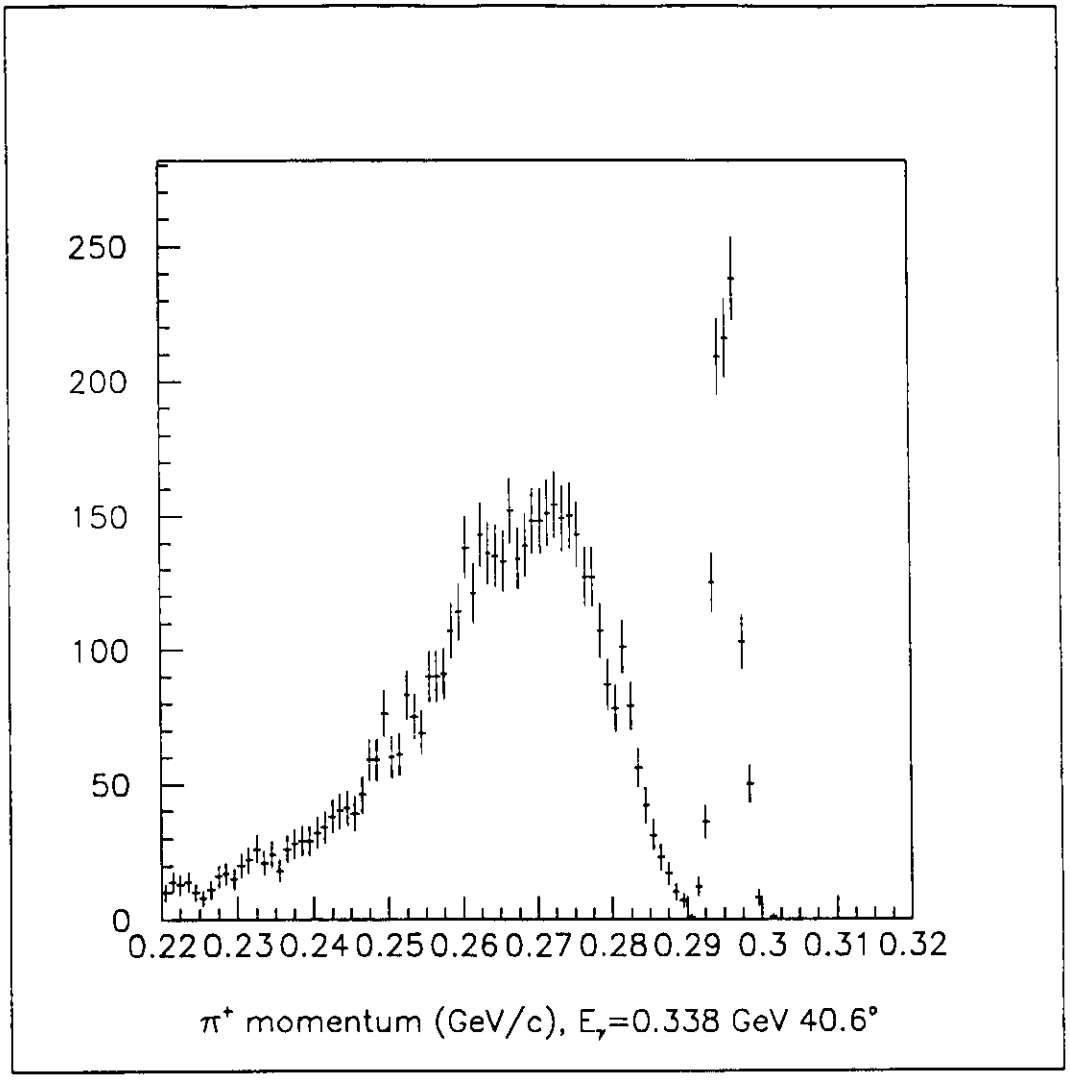

Figure 11. Pion momentum spectra for $E_\gamma = 338MeV$ at $\theta_\pi = 40.6$.

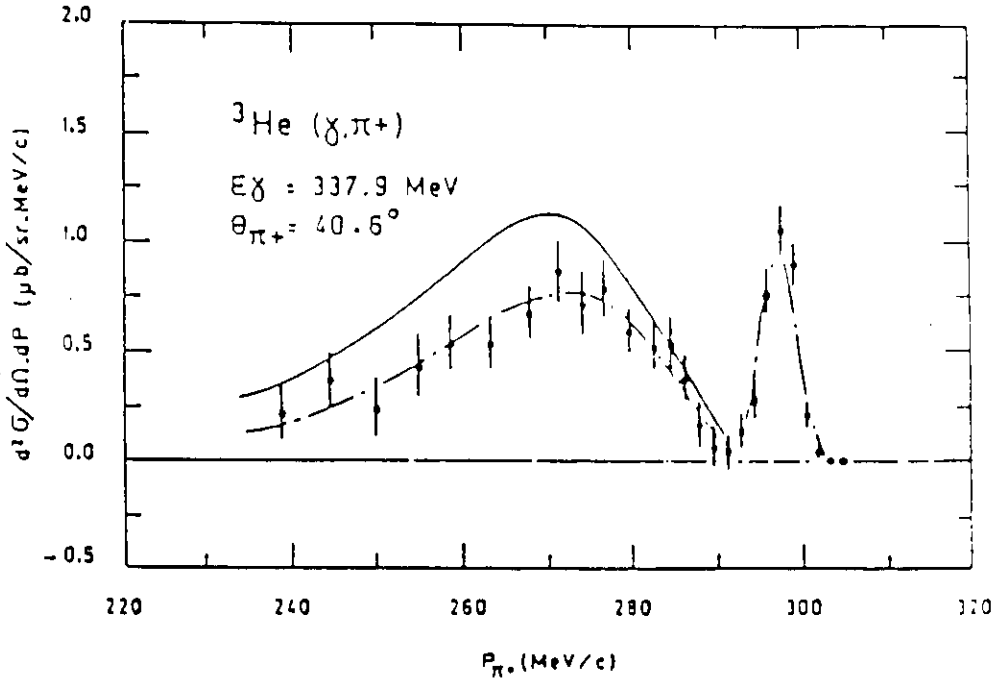

Figure 12. Pion momentum spectra for $E_\gamma = 338MeV$ at $\theta_\pi = 40.6$ from Saclay data.

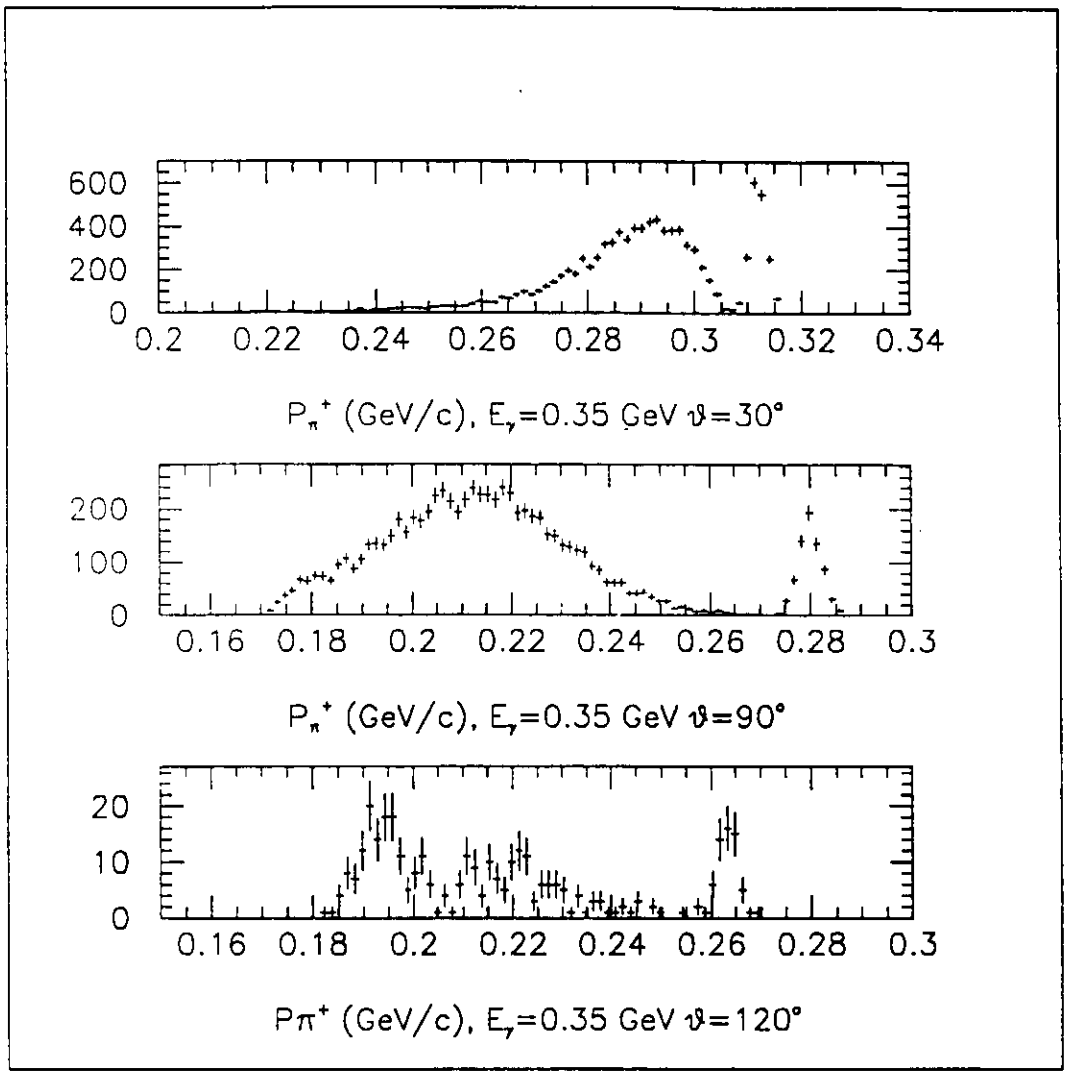

Figure 13. Pion momentum resolution for $E_\gamma = 350$ MeV and θ_π at 30, 90, 120 degree.

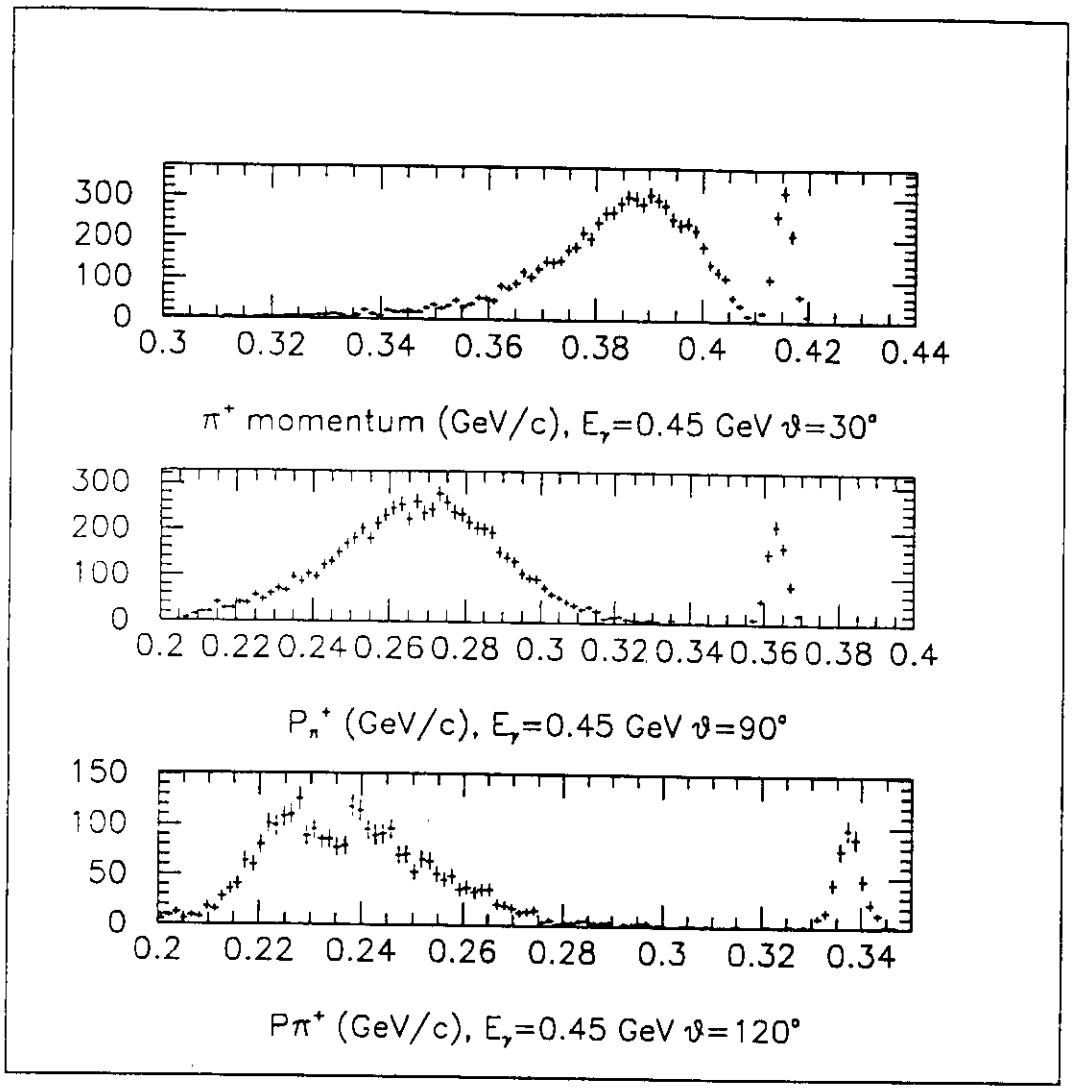

Figure 14. Pion momentum resolution for $E_\gamma = 450$ MeV and θ_π at 30, 90, 120 degree.

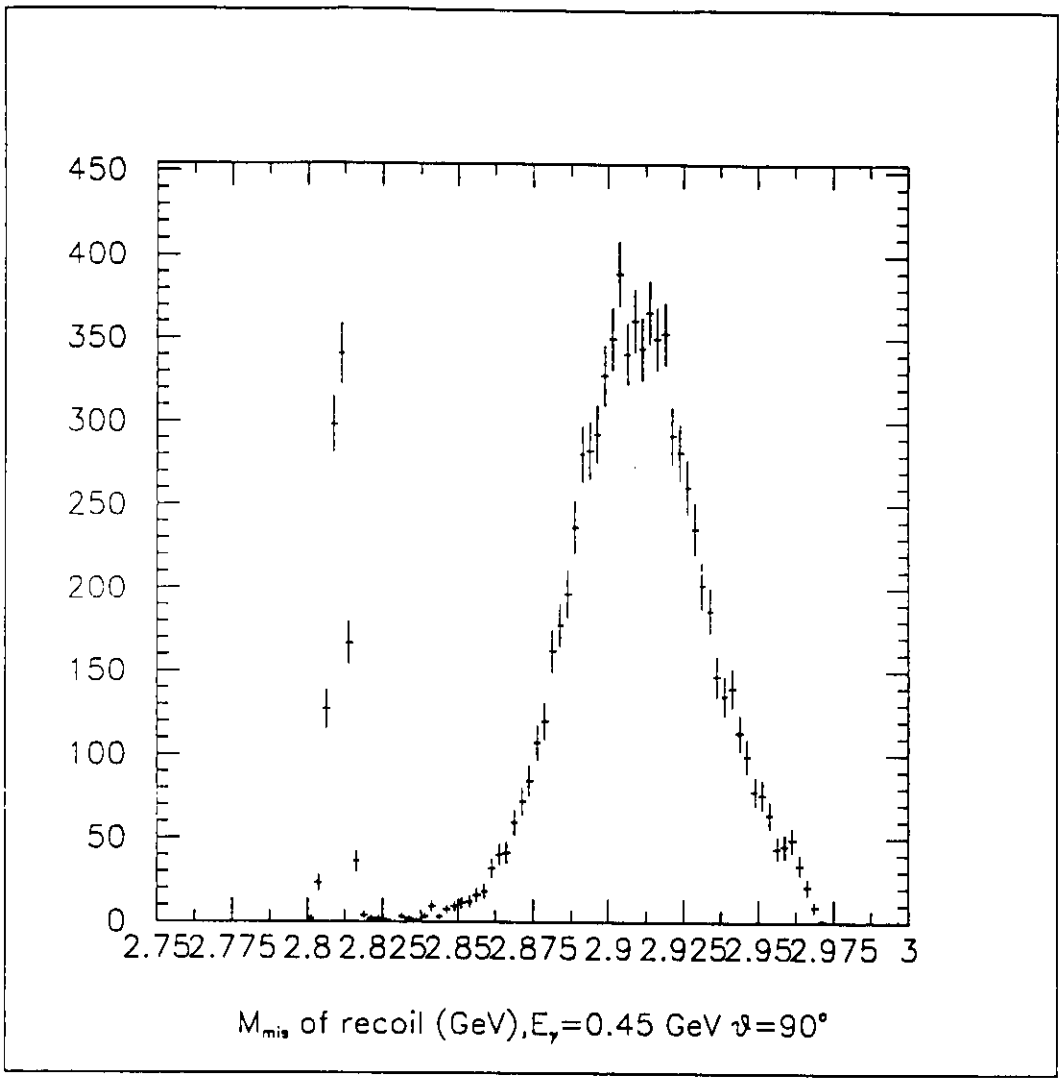

Figure 15. Missing mass spectrum for $E_\gamma = 450 MeV$ and $\theta_\pi = 90^o$.

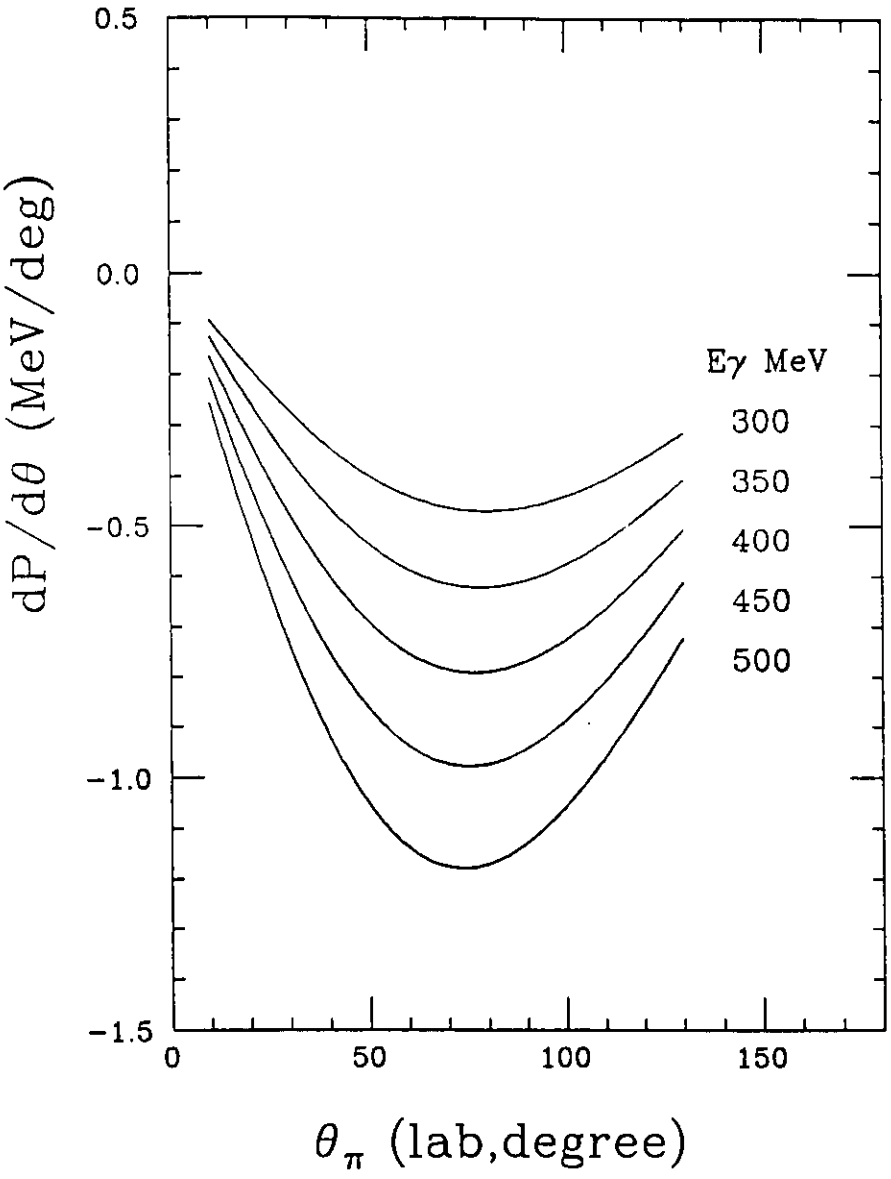

Figure 16. Derivative of pion momentum to angle θ_π for different E_γ's.

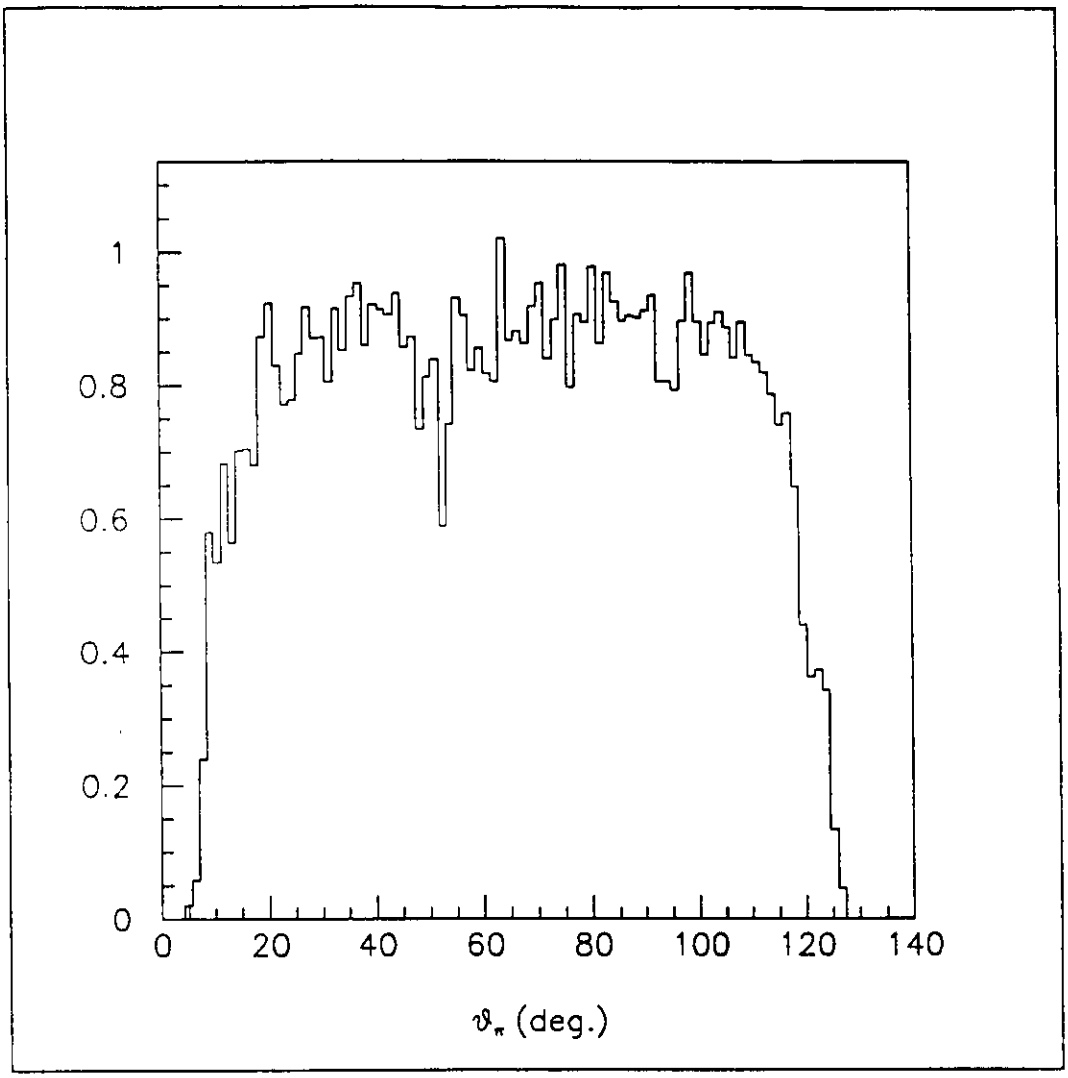

Figure 17. Acceptance of pion on polar angle at $E_\gamma = 450 MeV$.

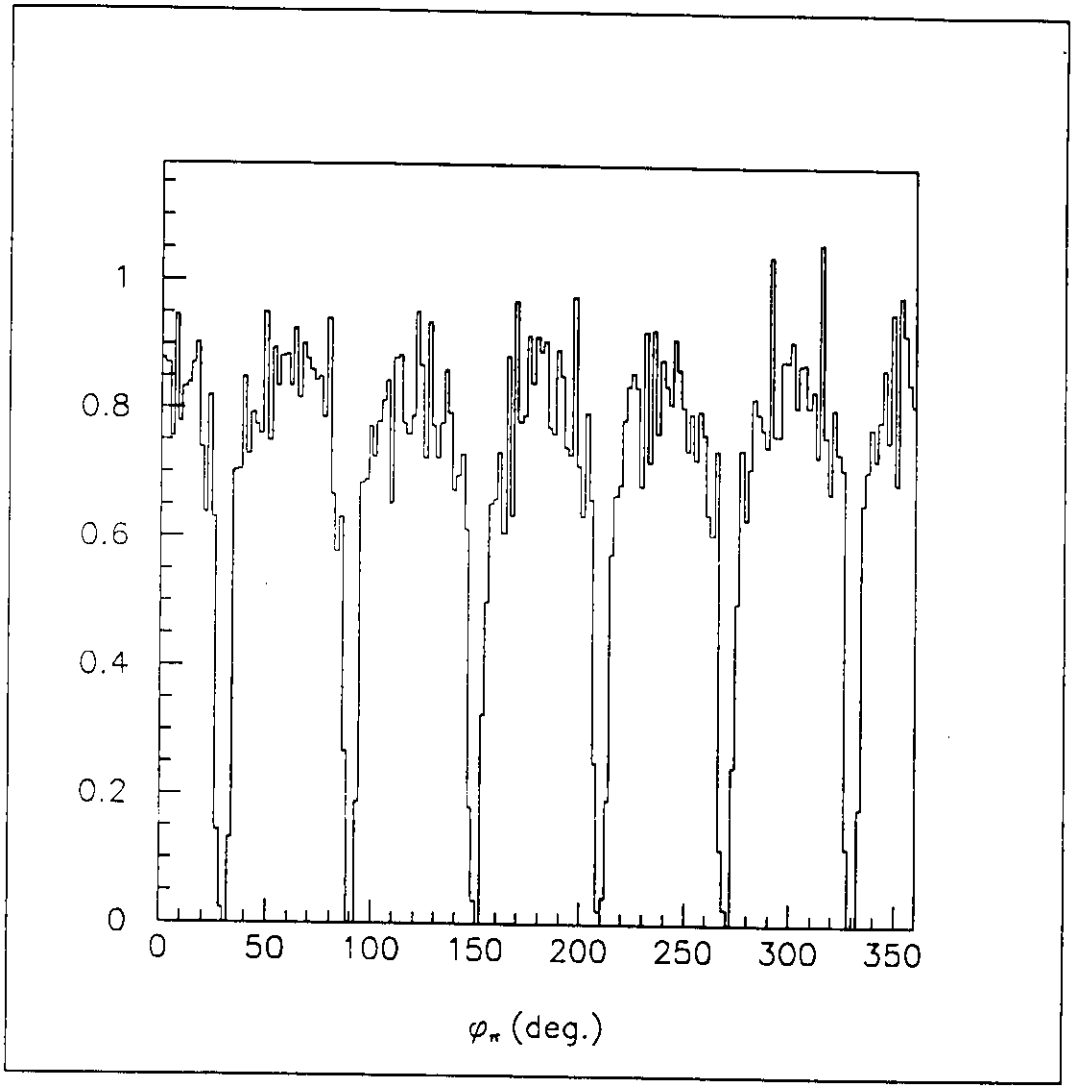

Figure 18. Acceptance of pion on azimuthal angle at $E_\gamma = 450 MeV$.

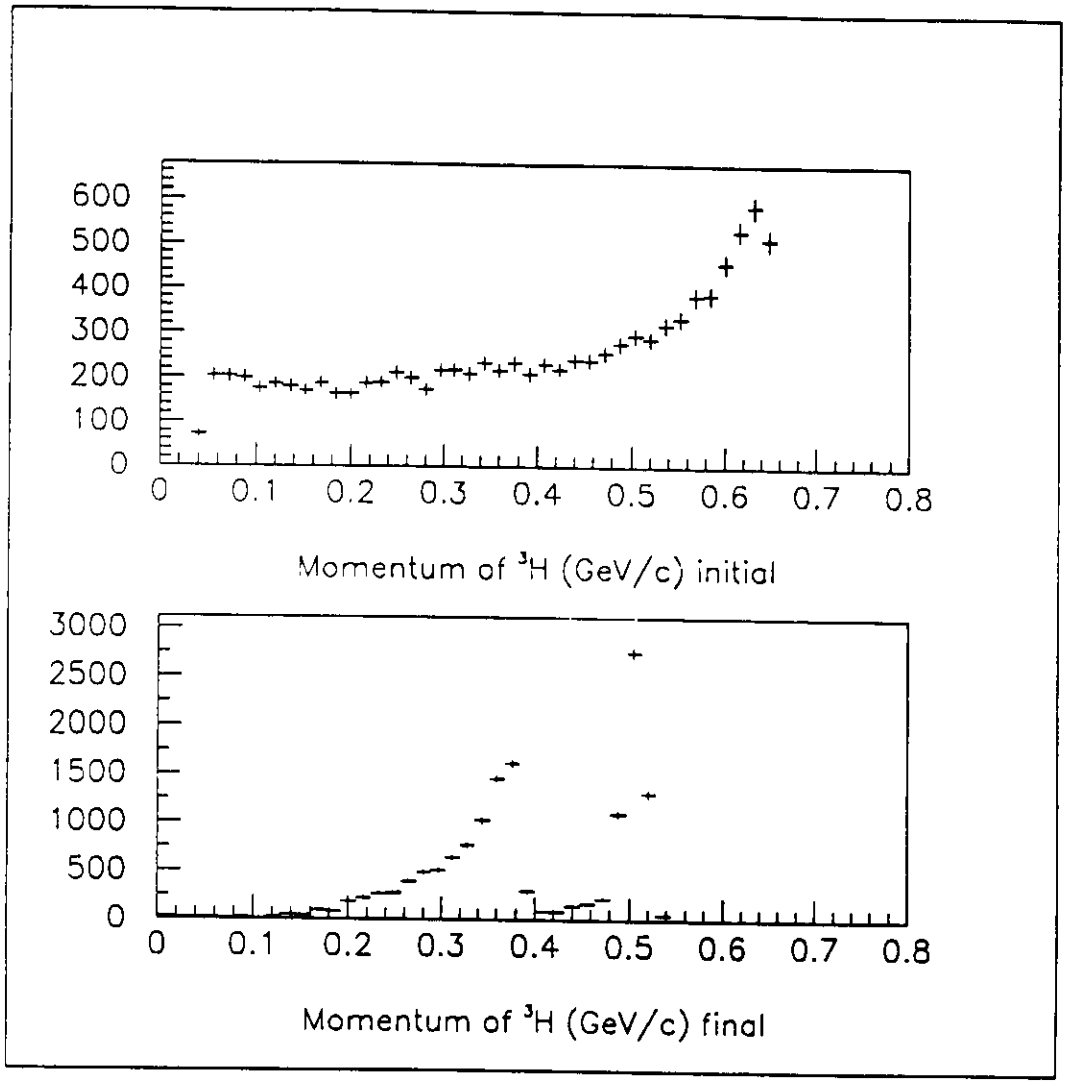

Figure 19. Acceptance of the recoiled momentum at $E_\gamma = 450MeV$, the discontinuity is resulted in from a sharp corner of the vertex detector in the forward direction.

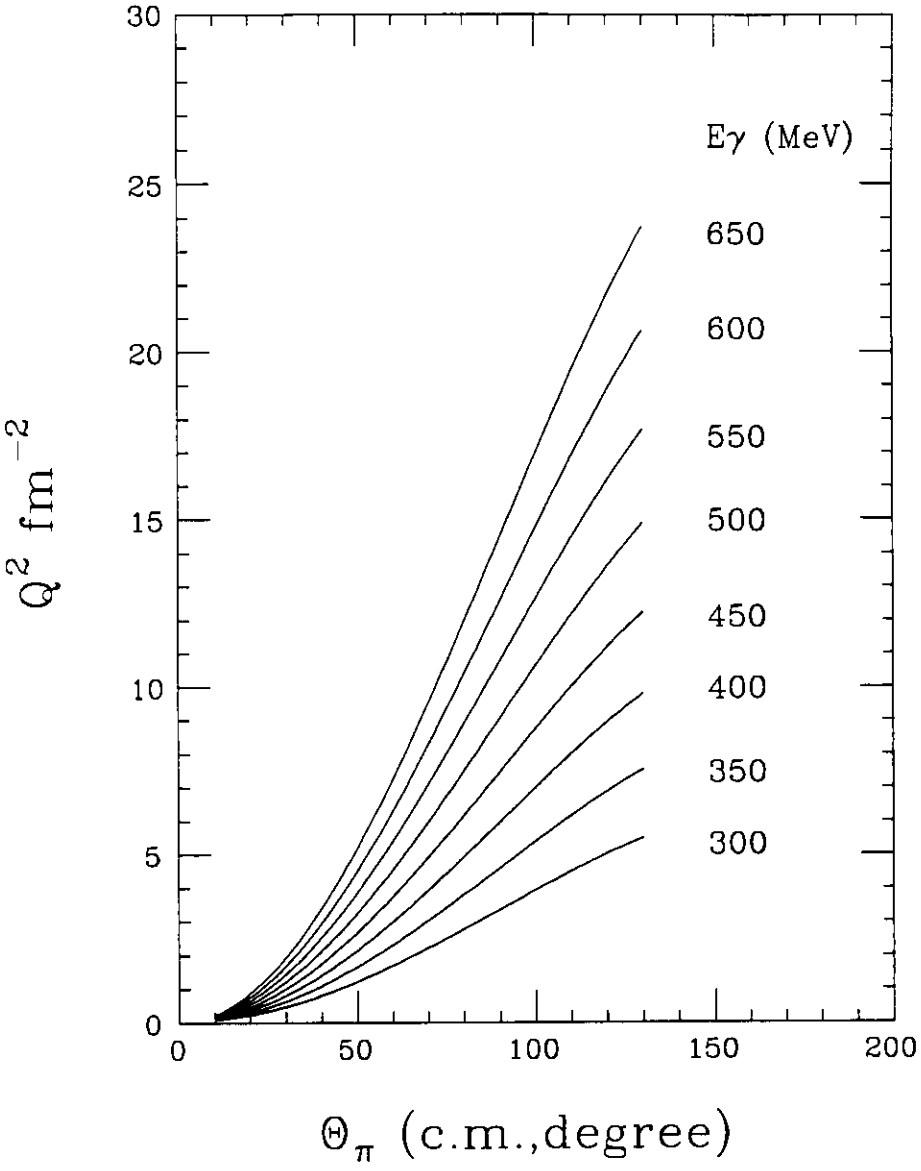

Figure 20. Q^2 dependence on angle Θ_π in c.m. system for different E_γ's.

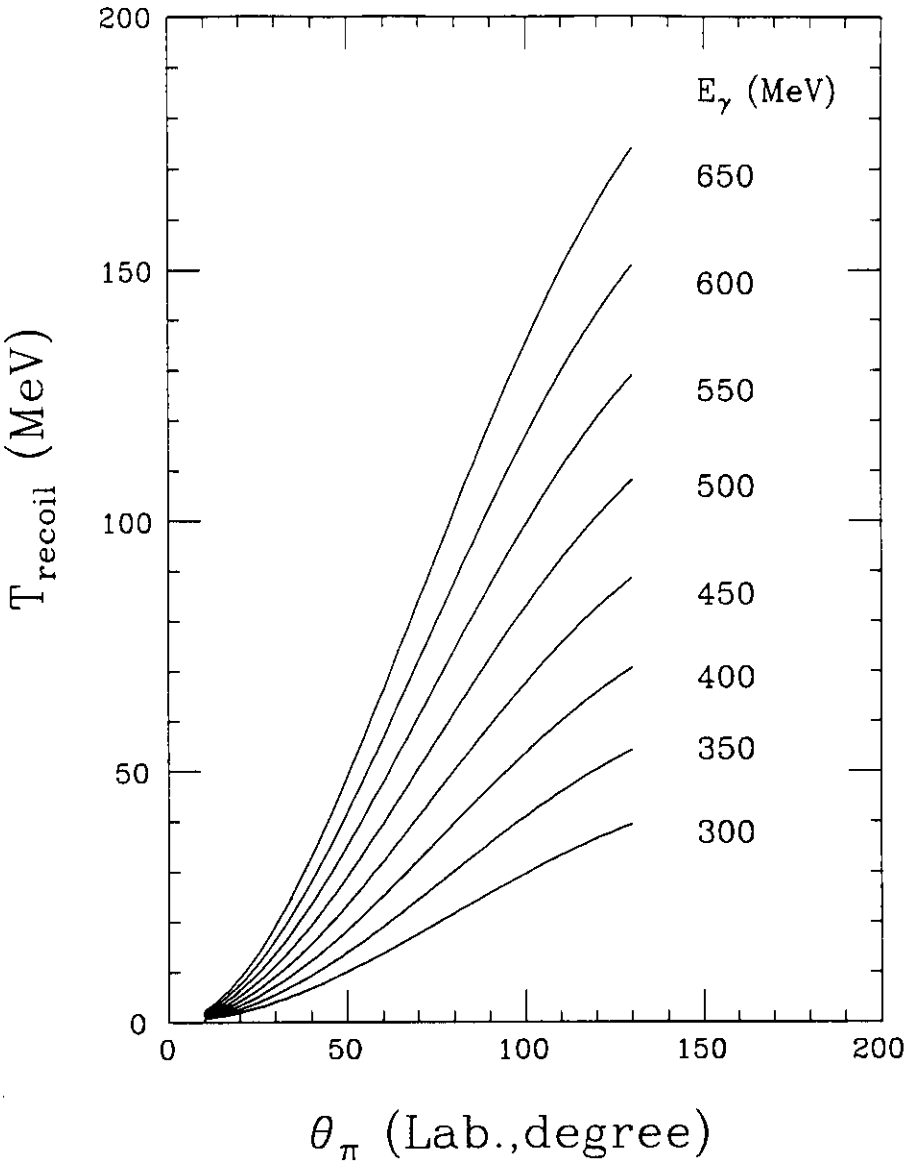

Figure 21. Recoil kinetic energy dependence on θ_π for different E_γ's.

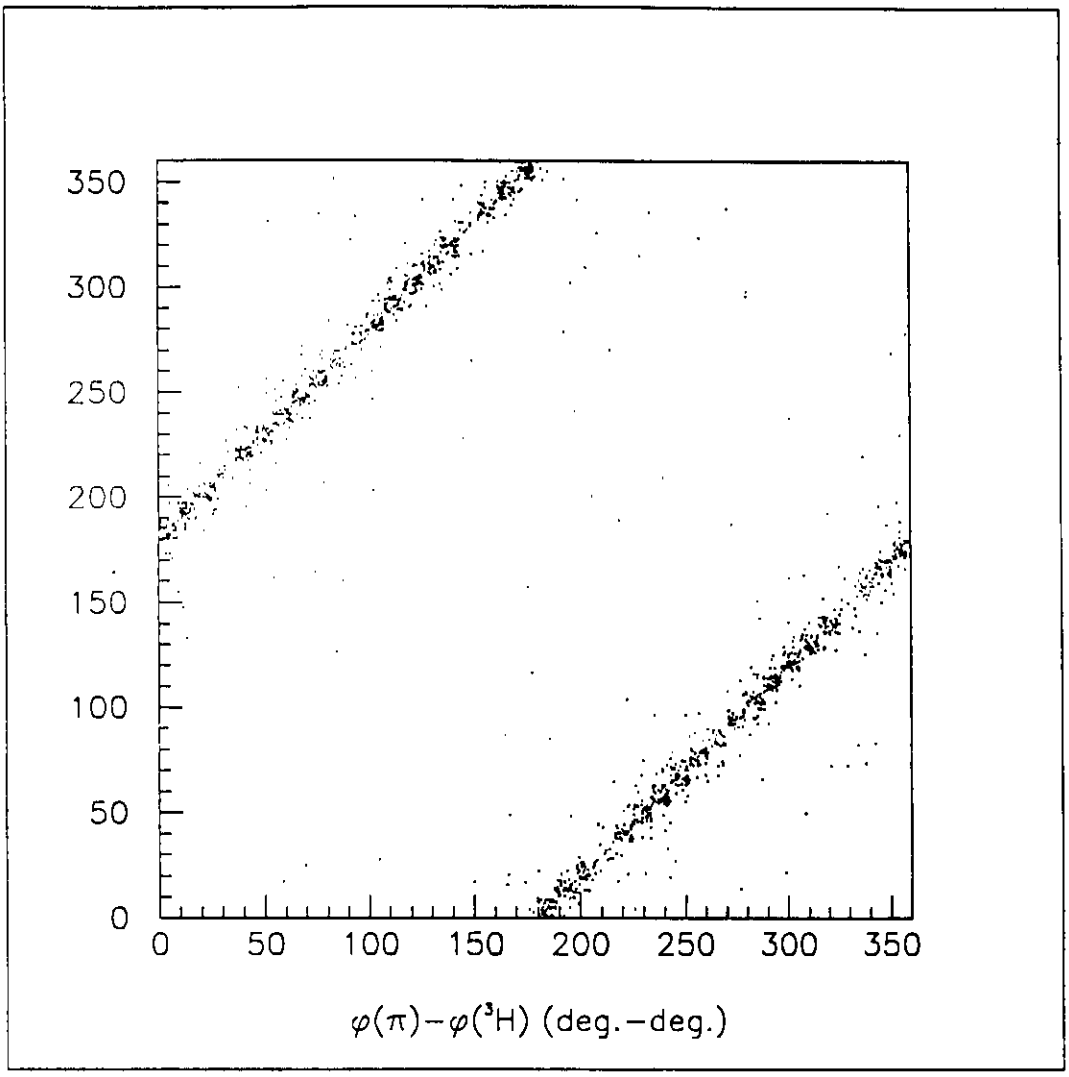

Figure 22. 2D histogram of ϕ_π and ϕ_{recoil}.